

Main Manuscript for

Wildfire smoke impacts on indoor air quality assessed using crowdsourced data in California

5 Yutong Liang^{a*}, Deep Sengupta^a, Mark J. Campmier^b, David M. Lunderberg^c, Joshua S. Apte^{b,d}, Allen H. Goldstein^{a,b*}

^aDepartment of Environmental Science, Policy, and Management, University of California at Berkeley, Berkeley, CA 94720, USA.

^bDepartment of Civil and Environmental Engineering, University of California at Berkeley, Berkeley, CA 94720, USA.

10 ^cDepartment of Chemistry, University of California at Berkeley, Berkeley, CA 94720, USA.

^dSchool of Public Health, University of California at Berkeley, Berkeley, CA 94720, USA.

*Yutong Liang or Allen H. Goldstein

Email: yutong.liang@berkeley.edu or ahg@berkeley.edu.

15 **Author Contributions:** Y.L., D.S., J.S.A. and A.H.G. designed research; Y.L., M.J.C. and D.M.L. performed the study; Y.L., M.J.C., D.S., J.S.A and A.H.G. jointly analyzed the data and wrote the article.

Competing Interest Statement: The authors declare no competing interests.

Keywords: biomass burning, PM_{2.5}, indoor air, exposure, low-cost PM_{2.5} sensors

20

This PDF file includes:

Main Text
Figures 1 to 5
Table 1

25

Abstract

Wildfires have become the dominant source of particulate matter ($\text{PM}_{2.5}$, $< 2.5 \mu\text{m}$ diameter) leading to unhealthy air quality index occurrences in the western United States. Since people mainly shelter indoors during wildfire smoke events, the infiltration of wildfire $\text{PM}_{2.5}$ into indoor environments is a key determinant of human exposure, and is potentially controllable with appropriate awareness, infrastructure investment, and public education. Using time-resolved observations outside and inside over 1400 buildings from the crowdsourced PurpleAir sensor network in California, we found that infiltration ratios (indoor $\text{PM}_{2.5}$ of outdoor origin/outdoor $\text{PM}_{2.5}$) were reduced on average from 0.4 during non-fire days to 0.2 during wildfire days. Even with reduced infiltration, mean indoor concentration of $\text{PM}_{2.5}$ nearly tripled during wildfire events, with lower infiltration in newer buildings and those utilizing air conditioning or filtration.

Significance Statement

Wildfires have become the dominant source of particulate matter in the western United States. Previous characterizations of exposure to wildfire smoke particles were based mainly on ambient concentration of $\text{PM}_{2.5}$. Since people mainly shelter indoors during smoke events, the infiltration of wildfire $\text{PM}_{2.5}$ into indoor environments determines exposure. We present analysis of infiltration of wildfire $\text{PM}_{2.5}$ into more than 1400 buildings in California using more than 2.4 million sensor-hours of data from the PurpleAir low-cost sensor network. Findings reveal that infiltration of $\text{PM}_{2.5}$ during wildfire days was substantially reduced compared with non-fire days, related to people's behavioral change. These results improve understanding of exposure to wildfire particles and facilitate informing the public about effective ways to reduce their exposure.

Introduction

Fine particulate matter (PM_{2.5}) air pollution is the single-largest environmental risk factor for human health and death in the United States (US) (1). Wildfires are a major source of PM_{2.5}, and are documented to cause adverse respiratory health effects and increased mortality (2). Toxicological and epidemiological studies suggest that PM_{2.5} from wildfires is more harmful to the respiratory system than equal doses of non-wildfire PM_{2.5} (3, 4). The number and magnitude of wildfires in the western US has increased in recent decades due to climate change and land management (5–7). Although the annual mean level of PM_{2.5} has substantially declined over this period following the implementation of extensive air quality policies to reduce emissions from controllable sources, the frequency and severity of smoke episodes with PM_{2.5} exceedances has increased sharply due to wildfires in the Pacific Northwest and California (8, 9). The annual mean PM_{2.5} in Northern California has increased since 2015 (*SI Appendix*, Fig. S1) due to massive seasonal fire events, and these events have become the dominant cause of PM_{2.5} exceedances.

People in the United States spend 87% of their time indoors (10). However, the protection against air pollutants of outdoor origin provided by buildings is commonly overlooked in air quality, epidemiologic, and risk assessment studies (11). To accurately characterize and reduce population exposures to wildfire PM_{2.5}, it is necessary to understand then optimize how buildings are used by their occupants to mitigate exposure. Previous estimations of indoor particles of outdoor origin typically relied on measurements from a limited number of buildings, and extrapolation of these measurements to other buildings based on the empirical infiltration and removal parameters (12, 13). However, such extrapolation is not applicable to wildfire events because it does not take into account the distribution of protection provided by buildings (including natural and mechanical ventilation) due to lack of data measuring infiltration under representative conditions. The infiltration of outdoor particles is dependent on people's behavior (11, 14, 15), which changes during wildfires (and in 2020 during the COVID-19 pandemic). Pollution levels during wildfire events, and knowledge of those pollution levels through available air quality data, directly impact human responses aimed at controlling the infiltration of outdoor PM_{2.5} including reducing ventilation, using

air conditioning, and using active filtration. Statistically robust observations of the variability of $PM_{2.5}$ infiltration during actual wildfire events across a broad cross-section of normally occupied residences provides the opportunity to understand the distribution of real infiltration rates affecting human exposure, and the factors controlling them, potentially informing guidance towards improvement.

Here, we exploit a recent trend in air quality sensing – public data from a network of ubiquitous crowdsourced low-cost $PM_{2.5}$ sensors – to characterize how indoor air quality during wildfire episodes is affected by buildings and their occupants. We demonstrate that buildings provide substantial protection against wildfire $PM_{2.5}$, and that behavioral responses of building occupants contribute to effective mitigation of wildfire smoke. Real-time $PM_{2.5}$ sensors based on aerosol light scattering have proliferated as easy-to-use and low-cost consumer devices in recent years, providing a novel opportunity to explore the indoor intrusion of wildfire $PM_{2.5}$. Among various devices available, the crowdsourced PurpleAir network has developed the most extensive public-facing network currently available. As of June 2, 2021, there are 15,885 publicly accessible active PurpleAir sensors reporting data from across the earth, 76% are outdoor (12,088), and 24% are indoor (3,797). Of these PurpleAir sensors, 57% are installed in California (9,072), split into 69% outdoor (6,273) and 31% indoor (2,799). As shown in Fig. 1, California accounts for 74% of all indoor PurpleAir sensors worldwide, with adoption increasing most rapidly following individual wildfire episodes, as noted by prior work (16). We focus here on analyzing the data from these sensors deployed across the metropolitan regions of San Francisco and Los Angeles, California, where the public adoption of indoor and outdoor PurpleAir sensors is especially high, at least partially in response to the high frequency of recent wildfire events. Analyses are presented for the wildfire season in the San Francisco Bay Area of Northern California (NC) during August-September 2020 (denoted NC 2020) and November 2018 (NC 2018), and for the Los Angeles area of Southern California (SC) in August-September 2020 (SC 2020). Maps of the measurement regions are provided in *SI Appendix*, Fig. S2 and S3. We analyzed the data from over 1,400 indoor sensors and their outdoor counterparts to characterize levels of and dynamics of indoor $PM_{2.5}$ and

the fraction of outdoor PM_{2.5} that entered buildings, comparing wildfire and non-fire periods. The vast majority (> 87%) of sensors in our dataset are in buildings that are unambiguously identified as residential. We mainly focus on residential buildings, which is facilitated by linking individual PurpleAir sensor locations with a dataset of detailed home property characteristics (Zillow).

Results and Discussion

PM_{2.5} inside and outside an example house. Fig. 2 displays the PM_{2.5} concentrations measured by an indoor sensor and its nearest outdoor counterpart on wildfire days and non-wildfire days (classified by whether the daily average PM_{2.5} level measured by the nearest EPA Air Quality Measurement Station was above or below 35 µg m⁻³). The outdoor PM_{2.5} concentration was clearly affected by wildfire plumes for August 14-28, September 6-15, and September 28-30. On fire days, the 10-min average outdoor PM_{2.5} exceeded 250 µg m⁻³ several times. The indoor concentration was more than doubled in these periods due to the infiltration of wildfire particles. We also observed peaks of indoor PM_{2.5} exceeding the outdoor PM_{2.5} even on the most polluted days. These peaks typically lasted between 1 hour and 4 hours, which match well with the characteristics of cooking/cleaning peaks, reported in studies such as Patel *et al.* and Tian *et al.* (17, 18). Fig. 2C shows the concentration profiles of indoor and outdoor PM_{2.5}, and 1D shows the outdoor PM_{2.5} and indoor PM_{2.5} with outdoor origins (after removal of identified indoor emission events). The infiltration of outdoor wildfire smoke caused the concentration of indoor PM_{2.5} to exceed 75 µg m⁻³ in this building occasionally (Fig. 2D).

Differences of infiltration on fire days and non-fire days. Taking all the buildings in the NC 2020 case into consideration, we found that the mean concentration of indoor PM_{2.5} nearly tripled on the fire days compared to the non-fire days due to the infiltration of outdoor smoke (Table 1, *SI Appendix*, Fig. S4). On the fire days, the average outdoor concentration of PM_{2.5} was more than 4 times the mean indoor PM_{2.5}. Fig. 3A displays the distribution of the mean indoor/outdoor PM_{2.5} ratio of each building on the fire days and the non-fire days. The average indoor/outdoor PM_{2.5} ratios for many buildings exceeded 1 due to indoor emission events, particularly on non-fire days.

On fire days, the majority of indoor $PM_{2.5}$ infiltrated from outdoors, but the indoor/outdoor $PM_{2.5}$ ratios were much lower because people closed their buildings and many also filtered their indoor air for protection from the smoke. Figure 3B shows the ratio of indoor $PM_{2.5}$ of outdoor origin to outdoor $PM_{2.5}$ (defined as the infiltration ratio). The infiltration factor (F_{in}) is the steady-state fraction of outdoor $PM_{2.5}$ that enters the indoor environment and remains suspended there (14). It quantifies the extent that the building provides protection against outdoor particles (11). For particulate matter, F_{in} can be obtained from the ratio of indoor/outdoor concentration when there are not additional indoor sources or loss processes (19, 20). On fire days ($PM_{2.5} > 35 \mu g m^{-3}$), due to the predominance of $PM_{2.5}$ of outdoor origin, the infiltration ratio approaches the infiltration factor. The infiltration factors of $PM_{2.5}$ for different buildings in NC 2020 have a geometric mean (GM) of 0.23 (0.16, 0.36 for 25th and 75th percentiles, same below). On non-fire days ($PM_{2.5} < 35 \mu g m^{-3}$), the GM infiltration ratio increases to 0.42 (0.35, 0.56), while on days with unhealthy air quality ($PM_{2.5} > 55.4 \mu g m^{-3}$), the GM infiltration ratio reduces to 0.19 (0.13, 0.31) (Table 1). However, around 18% of buildings had $PM_{2.5}$ infiltration factors above 0.4 on the fire days (Fig. 3B). Occupants of these exposure hotspot buildings could have experienced much higher levels of wildfire smoke. For context, infiltration factors of homes and commercial buildings measured in the US are usually above 0.5 (14, 21), and the infiltration factor of office buildings with 85% ASHRAE filters were predicted to be around 0.18 (22). The difference in mean infiltration ratio between fire days and non-fire days are most apparent in the daytime (*SI Appendix*, Fig. S5), consistent with more ventilation typically occurring during daytime (23). The lower infiltration factors for the buildings on fire days indicates the efficacy of reduced ventilation and enhanced removal of particles as people took measures to protect themselves from smoke exposure, and that more behavioral changes happened in daytime. Infiltration ratios of $PM_{2.5}$ were not significantly different between fire days and non-fire days in the SC 2020 case (Fig. 4), in contrast to the 2020 NC observations. This difference is probably because the hotter weather in Southern California caused more frequent use of air conditioning systems (and shutting windows), which is implied by a higher 2 pm mean indoor-outdoor temperature difference ($\sim 4^{\circ}C$) than buildings in the San Francisco Bay Area ($\sim 2^{\circ}C$).

Another possibility is that the PM_{2.5} pollution levels in the Greater Los Angeles area were not high enough to induce people to change their behaviors (*SI Appendix*, Fig. S6-S9).

Infiltration and building characteristics. Differences in fire-day infiltration ratios may also stem from differences in building characteristics. As shown in Table S4 in *SI Appendix*, buildings with fire-day infiltration ratio < 0.14 were widely distributed in the study area. However, buildings with fire-day infiltration ratio > 0.4 were mostly located in San Francisco where the climate is cooler and air conditioning is much less common. Buildings in California Climate Zone 12 (Northern California Central Valley) had lower infiltration ratios than any other climate zones in the San Francisco Bay Area (*SI Appendix*, Fig. S10). Due to the summer hot weather, substantial cooling is required for buildings in this zone (24). Air conditioning and associated filtration systems apparently decrease the indoor PM_{2.5} in those buildings. In addition, since the mid-late 1990s, most new residential buildings in the US are equipped with air conditioning systems (25). Since 2008, new buildings in California are mandated to have mechanical ventilation systems (26). Many of the newer buildings also have filtration systems (27). The changes in the building stock are apparent in the resulting data, as residences built after 2000 had significantly lower infiltration ratios on both fire days and non-fire days compared with older buildings (*SI Appendix*, Fig. S10), which is consistent with the findings of a recent wildfire smoke infiltration study in Seattle (28). We further classified the buildings in the NC 2020 case into cool buildings and hot buildings based on whether the 95th percentile indoor temperature reached 30°C. These cool buildings were more likely to have air conditioning systems on. As shown in *SI Appendix*, Fig. S11, the cool buildings have significantly lower fire-day infiltration ratios than the hot ones ($p < 0.01$), and around 17% of cool buildings had extremely low infiltration ratios (< 0.1). In sum, these results demonstrate that (i) this sensing and analysis approach yields findings in line with mechanistic plausibility (ii) and that the diversity of building characteristics within a region leads to substantial heterogeneity in the degree to which populations are protected indoors from wildfire PM_{2.5}.

Decay rate constants for PM_{2.5} were determined for all indoor observations using a box model (Equation 2). The difference in the decay rate constants of PM_{2.5} indoors further reveals why

the infiltration ratio was lower on fire days. Fig. 5 shows the distribution of mean total loss rate constant of $PM_{2.5}$ on fire days and non-fire days in the buildings. The mean and median total loss rate constants (λ_t) are 1.5 h^{-1} and 1.2 h^{-1} on fire days, and 2.2 h^{-1} and 1.9 h^{-1} on non-fire days, respectively. Comparing individual buildings on fire days and non-fire days, 67% of them have lower particle loss rate constants on fire days, indicating a high percentage of buildings whose occupants took effective action to reduce $PM_{2.5}$ infiltration. During the fire days, the decrease in air exchange rate exceeded the enhanced indoor filtration, making the loss rate smaller. Since the infiltration ratio (infiltration rate/total loss rate, $aP / (a + k_{loss})$) was also lower on fire days, it can be inferred that the infiltration rate (air exchange rate \times penetration factor, aP) was lower on fire days (Equations 1 and 3). We expect both air exchange rate and penetration factor to drop on fire days. Closure of windows and doors will lead to a lower air exchange rate. The usage of filtration systems on incoming air and closure of openings will lead to a lower penetration factor (12). For the SC 2020 case, the mean estimated particle loss rate constants (1.3 h^{-1} on fire days and 1.4 h^{-1} on non-fire days) are lower than in the San Francisco Bay Area (*SI Appendix*, Fig. S12), which further implies that a larger fraction of PurpleAir sensor owners in the Los Angeles area kept their windows/doors closed.

People are more likely to open the windows when the indoor temperature is higher than the outdoor temperature in summer (29, 30). In the NC 2020 and SC 2020 cases, the difference in daytime indoor/outdoor temperature alternated between positive and negative values (*SI Appendix*, Fig. S13). However, in the NC 2018 case, due to the colder outdoor temperatures in November, we infer that people probably closed their windows for a longer time, explaining the lower loss rate constants observed. This was expected to reduce the difference between the infiltration ratio on fire days and non-fire days. However, this ratio is still statistically significantly higher ($p < 0.05$) on fire days, which suggests the widespread application of filtration systems.

Our conclusions come with caveats. First, we treated each building as a well-mixed box, which assumes the indoor sensor measurement can represent the $PM_{2.5}$ levels of the entire building. Second, our algorithm to remove the indoor-source peaks could miss lower indoor

emission events. In addition, we assumed a universal quasi-linear response for all the PurpleAir sensors throughout the analysis period. Such treatment could lead to biases, but our results should still reflect the average trend. Indoor environments with PurpleAir sensors may not be representative of the entire distribution of buildings (details are provided in the *SI Appendix*). Adoption of PurpleAir sensors (at least ~200 US dollars per sensor) is higher among affluent people concerned about exposure to PM_{2.5}. Consistent with the expectation of an affluent “early-adopter” effect, PurpleAir owners live in homes with estimated average property values 21% greater than the median property value for their cities (*SI Appendix*, Table S3 and Fig. S14). The 2015 U.S. Residential Energy Consumption Survey shows that households with less than \$40,000 annual income are less likely to use air-conditioning equipment than other households (31). Low-income houses tend to be older, and they are shown to have larger leakage than other houses (32, 33). Lower-income households can therefore have disproportionately higher exposure to wildfire smoke. Finally, although we were not able to disentangle the influence of multiple regionally varying parameters (such as building type, floor area, property values) on penetration of wildfire smoke with the current distribution of indoor sensors, more extensive sensor adoption in coming years may allow future work to address this limitation.

This work demonstrates that crowdsourced environmental sensing can provide valuable information about how people are protecting themselves from the increasingly severe environmental hazard of wildfire smoke. We find that common adaptation measures, including reducing ventilation and active air filtration, effectively mitigate the average indoor exposures of all the buildings by 18% and 73% relative to indoor baseline and outdoor conditions, respectively. This work further suggests that such protective measures could be enhanced through public education to substantially mitigate indoor exposures at the population scale in the future. Given anticipated increases in wildfire smoke in coming decades, it is critical to evaluate these findings in other settings, including in lower-income communities and in other climate regions affected by wildfires. While our data imply that early adoption of crowdsourced indoor PurpleAir sensors seems to be propelled by wildfire events (Figure 1), gaining more broadly representative insight into the

distribution of indoor PM conditions might benefit from complementary approaches to disseminating these sensors, such as targeted deployments in lower-income communities. Overall, our results suggest the increasing ubiquity of indoor and outdoor air pollution sensors can aid in understanding exposures to episodic pollution sources such as wildfires.

Materials and Methods

Selection of Sensor Correction Models. The performance of low-cost PM_{2.5} sensors is dependent on humidity, temperature, particle size distribution and level of particulate matters (34–42). To evaluate the performance of the PurpleAir sensors against reference US EPA PM_{2.5}, we linked hourly average measurements from all 16 reference monitors in the study domain (for the entire study period) with surrounding (within 5 km) outdoor PurpleAir sensors, as detailed in the *SI Appendix* (section “Selection of Sensor Correction Models”, Figures S6-S9, Tables S1 and S2). We then evaluated the relationship between PM_{2.5} data from PurpleAir sensors and US EPA monitors for multiple calibration schemes in three categories: (i) previously reported calibration factors for wildfire smoke from the literature (35, 38), (ii) parsimonious empirical calibration relationships based on linear regression using this dataset, and (iii) a machine learning (random forest) based calibration scheme using this dataset. Our parsimonious ordinary least-square fit (correction factor = 0.53, intercept = 0) provided good agreement with the EPA measurements for this dataset, with $R^2 = 0.87$ and normalized root mean square error = 0.50. For the range of increasingly complex calibration models considering extra parameters for the PurpleAir vs. reference monitor that we developed, we found moderate further improvement to sensor precision and accuracy, but with qualitatively unchanged results (see *SI Appendix*). Accordingly, we rely on our no-intercept linear calibration equation for its more straightforward interpretability in our core analyses.

Decomposition of Indoor PM_{2.5} In addition to infiltration of PM_{2.5} from outdoors, cooking, cleaning and resuspension are the main sources of indoor PM_{2.5} (17, 18, 43). Prior to assessing the amount of indoor PM_{2.5} resulting from infiltration of wildfire smoke, we first identified and removed the events

(peaks) caused by indoor sources based on the magnitude and duration of indoor PM_{2.5} peaks. Details of the algorithm can be found in the *SI Appendix*.

Other QA and QC

270 As described in detailed QA/QC procedures in the *SI Appendix*, we sought to ensure appropriate sensor selection, and to exclude sensors that were likely mislabeled.

Mass Balance Model. We explored the dynamics of indoor PM_{2.5} with a well-mixed box model. When the indoor and outdoor particles are in steady state, and the indoor source is small, we have:

$$\frac{dC_{in}}{dt} = 0 = aPC_{out} - (a + k_{loss})C_{in} \Rightarrow F_{in} = \frac{C_{in}}{C_{out}} = \frac{aP}{a + k_{loss}} \quad [1]$$

275 where a is the air exchange rate, P is the penetration factor of particles, k_{loss} is the loss rate constant including deposition and indoor filtration. C_{in} and C_{out} are the indoor and outdoor concentrations, respectively (14, 19). F_{in} is the infiltration factor (which is close to the infiltration ratio).

Particle Loss Rate Constant Calculation. After major indoor emission events, the indoor concentration of PM_{2.5} will decay following:

$$280 \quad \frac{dC_{in}}{dt} = -(a + k_{loss})C_{in} \quad [2]$$

Therefore, $(a + k_{loss})$ can be estimated by fitting the curve of $C_{in}(t)$ (44). We define the total indoor particle loss rate constant (λ_t) as:

$$\lambda_t = a + k_{loss} \quad [3]$$

Details of the derivation of these equations and the algorithms are provided in the *SI Appendix*.

285 **Building information.** Property data were obtained by matching coordinates associated with the PurpleAir sensors to addresses. The list of addresses was then inputted to Zillow, a publicly accessible website to find the publicly available building information such as building age and livable area. Zillow uses existing building information and a proprietary algorithm to derive an estimate of the current (as of December 2020) price of the home or apartment. More details are
290 provided in the *SI Appendix*.

Data availability Data used in this work can be freely downloaded from the PurpleAir and EPA websites (links are provided in the *SI Appendix*).

Acknowledgments

295 The authors acknowledge Tongshu Zheng at Duke University for his advice on processing the data from the PurpleAir sensors. We thank the owners of PurpleAir sensors who generously shared the measurement data online. This work was supported by the National Oceanic and Atmospheric Administration (NOAA) Climate Program Office's AC4 program (Award No. NA16OAR4310107) and California Air Resources Board (Award No. 19RD008). This publication was also developed
300 as part of the Center for Air, Climate and Energy Solutions (CACES), which was supported under Assistance Agreement No. R835873 awarded by the U.S. Environmental Protection Agency. It has not been formally reviewed by EPA. The views expressed in this document are solely those of authors and do not necessarily reflect those of the Agency. EPA does not endorse any products or commercial services mentioned in this publication.

305 **References**

1. GBD 2019 Diseases and Injuries Collaborators, Global burden of 369 diseases and injuries in 204 countries and territories, 1990–2019: a systematic analysis for the Global Burden of Disease Study 2019. *Lancet* **396**, 1204–1222 (2020).
- 310 2. C. E. Reid, *et al.*, Critical review of health impacts of wildfire smoke exposure. *Environ. Health Perspect.* **124**, 1334–1343 (2016).
3. T. C. Wegesser, K. E. Pinkerton, J. A. Last, California wildfires of 2008: Coarse and fine particulate matter toxicity. *Environ. Health Perspect.* **117**, 893–897 (2009).
- 315 4. R. Aguilera, T. Corringham, A. Gershunov, T. Benmarhnia, Wildfire smoke impacts respiratory health more than fine particles from other sources: observational evidence from Southern California. *Nat. Commun.* **12** (2021).
5. P. E. Dennison, S. C. Brewer, J. D. Arnold, M. A. Moritz, Large wildfire trends in the western United States, 1984–2011. *Geophys. Res. Lett.* **41**, 2928–2933 (2014).
- 320 6. J. T. Abatzoglou, A. P. Williams, Impact of anthropogenic climate change on wildfire across western US forests. *Proc. Natl. Acad. Sci. U. S. A.* **113**, 11770–11775 (2016).
7. A. L. Westerling, Warming and Earlier Spring Increase Western U.S. Forest Wildfire Activity. *Science*. **313**, 940–943 (2006).
8. K. O'Dell, B. Ford, E. V. Fischer, J. R. Pierce, Contribution of Wildland-Fire Smoke to US PM 2.5 and Its Influence on Recent Trends. *Environ. Sci. Technol.* **53**, 1797–1804 (2019).
- 325 9. C. D. McClure, D. A. Jaffe, US particulate matter air quality improves except in wildfire-prone areas. *Proc. Natl. Acad. Sci. U. S. A.* **115**, 7901–7906 (2018).
10. N. E. Klepeis, *et al.*, The National Human Activity Pattern Survey (NHAPS): A resource for assessing exposure to environmental pollutants. *J. Expo. Anal. Environ. Epidemiol.* **11**, 231–252 (2001).
- 330 11. A. H. Goldstein, W. W. Nazaroff, C. J. Weschler, J. Williams, How Do Indoor Environments Affect Air Pollution Exposure? *Environ. Sci. Technol.* **55**, 100–108 (2021).
12. E. Diapouli, A. Chaloulakou, P. Koutrakis, Estimating the concentration of indoor particles of outdoor origin: A review. *J. Air Waste Manag. Assoc.* **63**, 1113–1129 (2013).
- 335 13. K. K. Barkjohn, *et al.*, Real-time measurements of PM2.5 and ozone to assess the effectiveness of residential indoor air filtration in Shanghai homes. *Indoor Air* **31**, 74–87 (2021).
14. C. Chen, B. Zhao, Review of relationship between indoor and outdoor particles: I/O ratio, infiltration factor and penetration factor. *Atmos. Environ.* **45**, 275–288 (2011).
- 340 15. L. K. Baxter, C. Stallings, L. Smith, J. Burke, Probabilistic estimation of residential air exchange rates for population-based human exposure modeling. *J. Expo. Sci. Environ. Epidemiol.* **27**, 227–234 (2017).
16. B. Krebs, J. Burney, J. G. Zivin, M. Neidell, Using Crowd-Sourced Data to Assess the Temporal and Spatial Relationship between Indoor and Outdoor Particulate Matter. *Environ. Sci. Technol.* **55**, 6107–6115 (2021).

- 345 17. S. Patel, *et al.*, Indoor Particulate Matter during HOMEChem: Concentrations, Size Distributions, and Exposures. *Environ. Sci. Technol.* **54**, 7107–7116 (2020).
18. Y. Tian, *et al.*, Indoor emissions of total and fluorescent supermicron particles during HOMEChem. *Indoor Air* **31**, 88–98 (2021).
- 350 19. L. Wallace, R. Williams, Use of personal-indoor-outdoor sulfur concentrations to estimate the infiltration factor and outdoor exposure factor for individual homes and persons. *Environ. Sci. Technol.* **39**, 1707–1714 (2005).
20. S. Bhangar, N. A. Mullen, S. V Hering, N. M. Kreisberg, W. W. Nazaroff, Ultrafine particle concentrations and exposures in seven residences in northern California. *Indoor Air* **21**, 132–144 (2011).
- 355 21. X. Wu, M. G. Apte, D. H. Bennett, Indoor particle levels in small- and medium-sized commercial buildings in California. *Environ. Sci. Technol.* **46**, 12355–12363 (2012).
22. W. J. Riley, T. E. McKone, A. C. K. Lai, W. W. Nazaroff, Indoor particulate matter of outdoor origin: Importance of size-dependent removal mechanisms. *Environ. Sci. Technol.* **36**, 200–207 (2002).
- 360 23. H. Erhorn, Influence of meteorological conditions on inhabitants' behaviour in dwellings with mechanical ventilation. *Energy Build.* **11**, 267–275 (1988).
24. Pacific Energy Center, "Pacific Energy Center's Guide to California Climate Zones and Bioclimatic Design" (2006) (January 26, 2021).
25. U.S. Census Bureau, "Characteristics of New Housing" (2019) (February 8, 2021).
- 365 26. California Energy Commission, 2008 Building Energy Efficiency Standards (2008).
27. B. C. Singer, W. R. Chan, Y. S. Kim, F. J. Offermann, I. S. Walker, Indoor air quality in California homes with code-required mechanical ventilation. *Indoor Air* **30**, 885–899 (2020).
- 370 28. J. Xiang, *et al.*, Field measurements of PM_{2.5} infiltration factor and portable air cleaner effectiveness during wildfire episodes in US residences. *Sci. Total Environ.* **773**, 145642 (2021).
29. D. Yan, *et al.*, Occupant behavior modeling for building performance simulation: Current state and future challenges. *Energy Build.* **107**, 264–278 (2015).
- 375 30. R. Andersen, V. Fabi, J. Toftum, S. P. Corngati, B. W. Olesen, Window opening behaviour modelled from measurements in Danish dwellings. *Build. Environ.* **69**, 101–113 (2013).
31. EIA, Residential Energy Consumption Survey (RECS). 2 (2013).
32. W. R. Chan, W. W. Nazaroff, P. N. Price, M. D. Sohn, A. J. Gadgil, Analyzing a database of residential air leakage in the United States. *Atmos. Environ.* **39**, 3445–3455 (2005).
- 380 33. G. Adamkiewicz, *et al.*, Moving environmental justice indoors: Understanding structural influences on residential exposure patterns in low-income communities. *Am. J. Public Health* **101** (2011).
34. W. W. Delp, B. C. Singer, Wildfire smoke adjustment factors for low-cost and professional PM_{2.5} monitors with optical sensors. *Sensors* **20**, 1–21 (2020).

- 385 35. A. L. Holder, *et al.*, Field evaluation of low-cost particulate matter sensors for measuring wildfire smoke. *Sensors* **20**, 1–17 (2020).
36. K. Ardon-Dryer, Y. Dryer, J. N. Williams, N. Moghimi, Measurements of PM_{2.5} with PurpleAir under atmospheric conditions. *Atmos. Meas. Tech.* **13**, 5441–5458 (2020).
37. T. Zheng, *et al.*, Field evaluation of low-cost particulate matter sensors in high-and low-concentration environments. *Atmos. Meas. Tech.* **11**, 4823–4846 (2018).
- 390 38. K. K. Barkjohn, A. Holder, S. Frederick, G. Hagler, A. Clements, PurpleAir PM_{2.5} U.S. Correction and Performance During Smoke Events in *International Smoke Symposium*, (2020).
- 395 39. J. Bi, A. Wildani, H. H. Chang, Y. Liu, Incorporating Low-Cost Sensor Measurements into High-Resolution PM_{2.5} Modeling at a Large Spatial Scale. *Environ. Sci. Technol.* **54**, 2152–2162 (2020).
40. J. Kuula, *et al.*, Laboratory evaluation of particle-size selectivity of optical low-cost particulate matter sensors. *Atmos. Meas. Tech* **13**, 2413–2423 (2020).
41. K. K. Barkjohn, B. Gantt, A. L. Clements, Development and application of a United States-wide correction for PM 2.5 data collected with the PurpleAir sensor. *Atmos. Meas. Tech* **14**, 4617–4637 (2021).
- 400 42. T. Zheng, *et al.*, Gaussian Process regression model for dynamically calibrating a wireless low-cost particulate matter sensor network in Delhi. *Atmos. Meas. Tech.* **12**, 5161–5181 (2019).
- 405 43. A. R. Ferro, R. J. Kopperud, L. M. Hildemann, Source Strengths for Indoor Human Activities that Resuspend Particulate Matter. *Environ. Sci. Technol.* **38**, 1759–1764 (2004).
44. B. Stephens, J. A. Siegel, Penetration of ambient submicron particles into single-family residences and associations with building characteristics. *Indoor Air* **22**, 501–513 (2012).

410 **Figures and Tables**

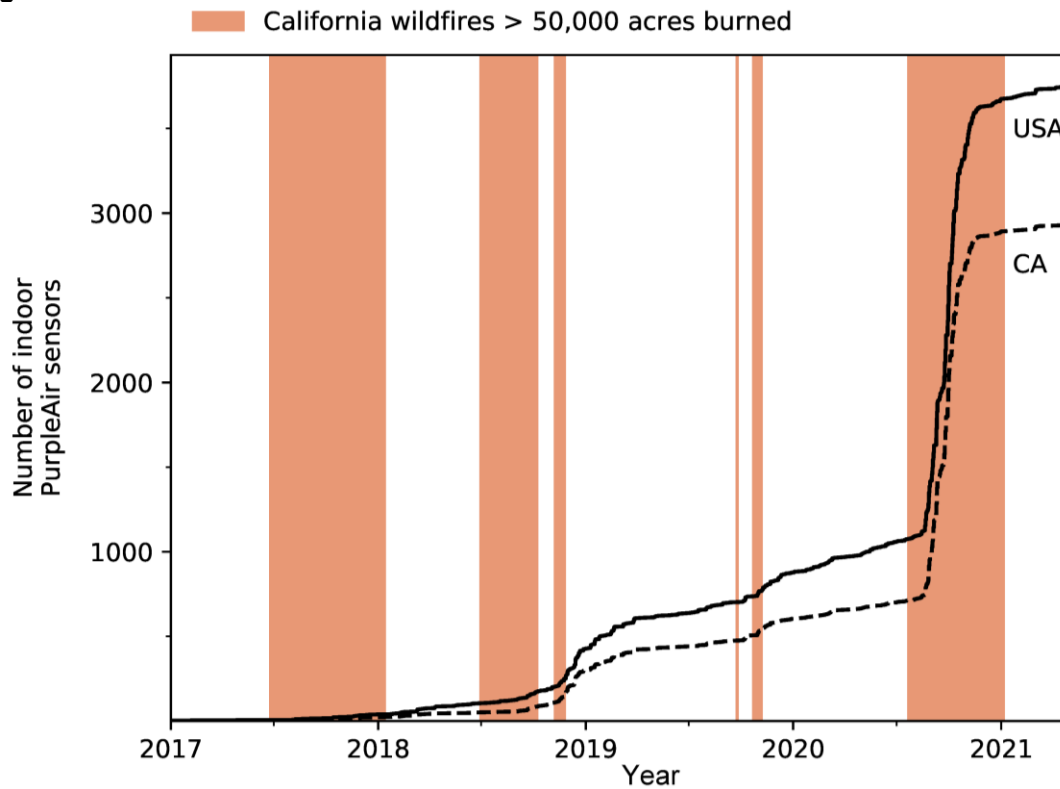


Figure 1. Number of publicly accessible indoor PurpleAir sensors in the United States and California. Shadings show major wildfire periods (start date to containment date of fires with > 50,000 total acres burned) in California. Wildfire periods are from Cal Fire website

415 (<https://www.fire.ca.gov/incidents/>).

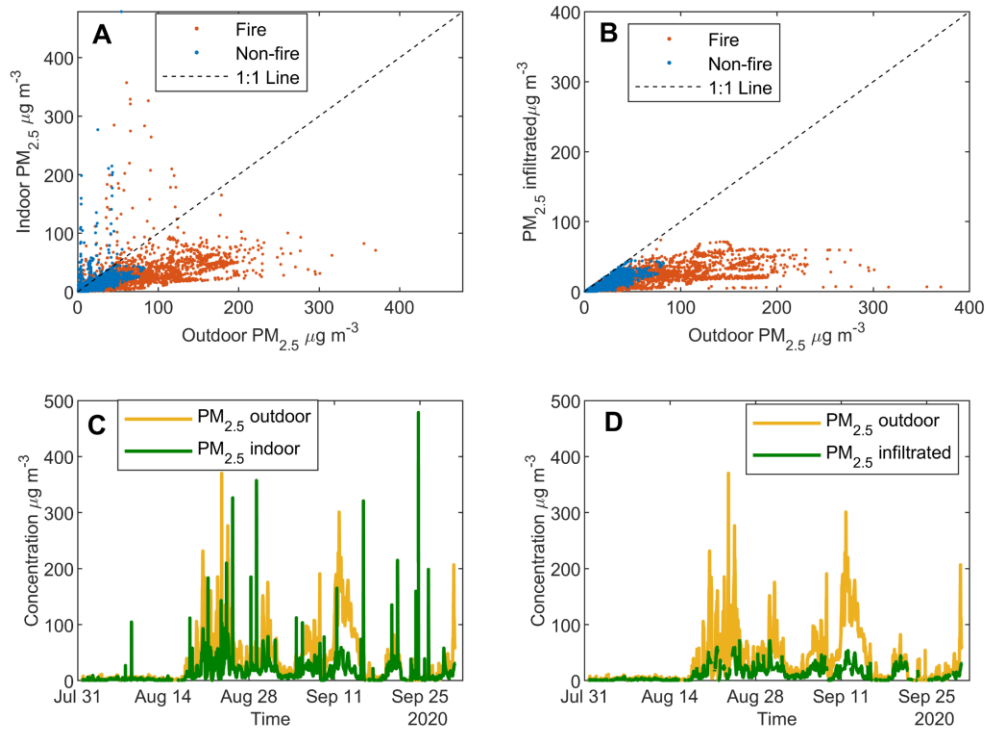


Figure 2. Relationship of indoor and outdoor PM_{2.5} for an example house **(A)** Scatterplots of calibrated PM_{2.5} measured at 10-min resolution by an indoor PurpleAir sensor against the nearest outdoor PurpleAir measurement, differentiating fire days (red) and non-fire days (blue), illustrative of the levels of PM_{2.5} pollution of buildings in the NC 2020 case. **(B)** Scatterplots of calibrated indoor PM_{2.5} of outdoor origin against outdoor PM_{2.5}. **(C)** Concentration time profile of calibrated indoor and outdoor PM_{2.5} measured by the two sensors. **(D)** Concentration time profile of calibrated infiltrated PM_{2.5} and outdoor PM_{2.5}. The figures demonstrate the indoor PM_{2.5} were clearly affected by the outdoor smoke, and our algorithm can effectively remove the indoor peaks due to indoor emissions.

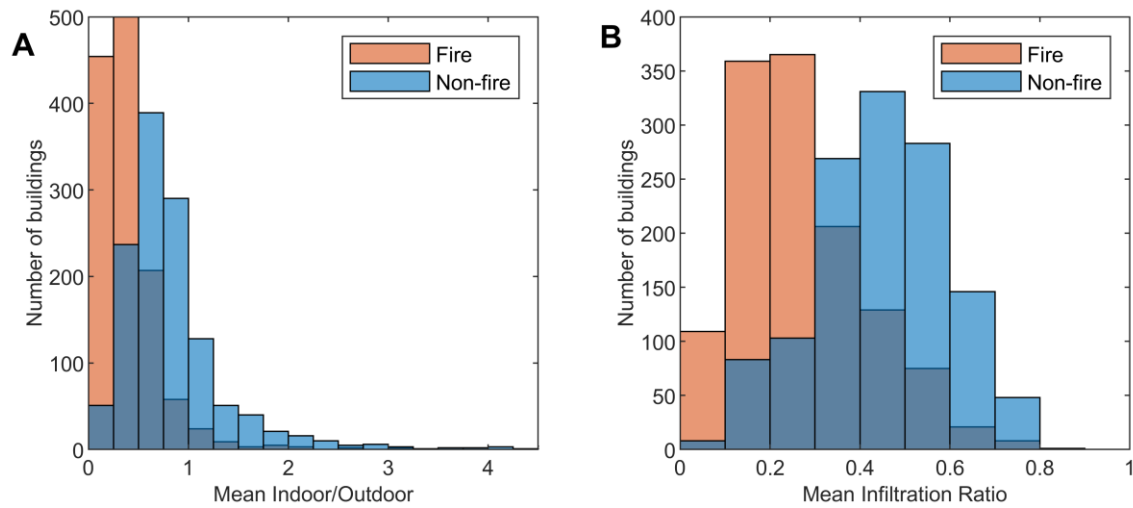


Figure 3. Distribution of the indoor/outdoor ratio and the infiltration ratio in the San Francisco Bay Area in August and September 2020. **(A)** Mean Indoor/Outdoor $PM_{2.5}$ ratio of buildings during fire days and non-fire days and **(B)** mean infiltrated $PM_{2.5}$ /Outdoor $PM_{2.5}$ ratio of buildings during fire days and non-fire days. Buildings have lower indoor/outdoor $PM_{2.5}$ ratio and infiltration ratio on fire-days.

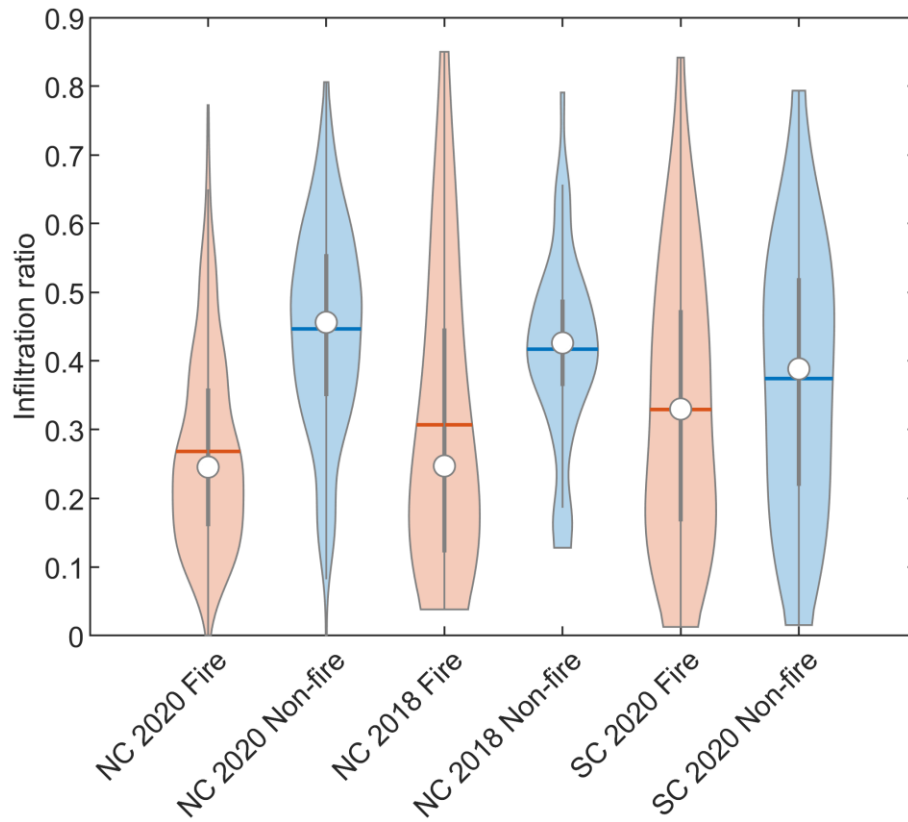
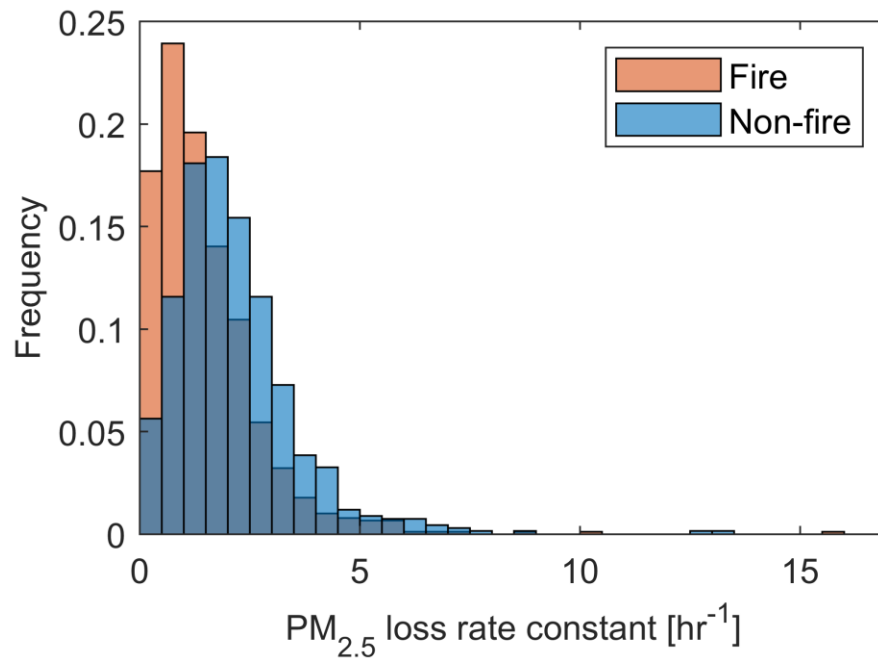


Figure 4. Violin plots of particle infiltration ratios during fire and non-fire periods. N = 1274 buildings, 2.1×10^6 sensor-hours for NC 2020, N = 115 buildings, 2.8×10^5 sensor-hours for SC 2020 and N = 52 buildings, 4.4×10^4 sensor-hours for NC 2018. Each violin plot shows the probability density of the infiltration ratio and a boxplot of interquartile range with whiskers extended to 1.5 times the interquartile range. Circles indicate the median, and horizontal lines indicate the mean.



445 **Figure 5.** Frequency distribution of indoor PM_{2.5} total loss rate constants (λ_t) in buildings in the San Francisco Bay Area on the fire days and non-fire days in August-September 2020 (decay peaks were found in $N = 1000$ buildings). A reduced total PM_{2.5} loss rate constant on the fire days indicates a reduction in ventilation.

Table 1. Statistics of the concentration indoor/outdoor ratios for buildings with PurpleAir sensors in August-September 2020 in the San Francisco Bay Area (35 $\mu\text{g m}^{-3}$ daily average $\text{PM}_{2.5}$ concentration measured at the nearest EPA measurement site was used as the threshold for fire days and non-fire days). $N = 1274$. Unhealthy days are defined as days with daily average EPA $\text{PM}_{2.5}$ concentration above 55.4 $\mu\text{g/m}^3$. GM = Geometric Mean, GSD = Geometric Standard Deviation.

	Mean outdoor conc $\mu\text{g m}^{-3}$	Mean indoor conc $\mu\text{g m}^{-3}$		Indoor/outdoor ratio		Infiltration ratio	
	Mean \pm s.d.	Mean \pm s.d.	GM, GSD	Mean \pm s.d.	GM, GSD	Mean \pm s.d.	GM, GSD
Non-fire days	9.1 \pm 4.0	4.1 \pm 2.5	3.7, 1.6	0.90 \pm 0.88	0.73, 1.8	0.45 \pm 0.15	0.42, 1.5
Fire days	45.4 \pm 17.0	11.1 \pm 8.3	8.9, 2.0	0.41 \pm 0.44	0.31, 2.1	0.27 \pm 0.14	0.23, 1.8
Unhealthy days	61.2 \pm 20.5	13.5 \pm 10.6	10.3, 2.1	0.31 \pm 0.42	0.23, 2.1	0.23 \pm 0.14	0.19, 1.9

Quantile-quantile plots (*SI Appendix*, Fig. S4) show the mean concentration of indoor $\text{PM}_{2.5}$ in all the buildings can be satisfactorily described by the Weibull distribution. Parameters of the Weibull fit are shown in Table S5 in the *SI Appendix*. Parameters of the SC 2020 and NC 2018 cases are not shown here due to the small sample sizes, which are less representative of all the buildings in these areas at that time.

460 **Supplementary Information for**

Wildfire smoke impacts on indoor air quality assessed using crowdsourced data in California

465 Yutong Liang^{a*}, Deep Sengupta^a, Mark J. Campmier^b, David M. Lunderberg^c, Joshua S. Apte^{b,d}, , Allen H. Goldstein^{a,b*}

^aDepartment of Environmental Science, Policy, and Management, University of California at Berkeley, Berkeley, CA 94720, USA.

470 ^bDepartment of Civil and Environmental Engineering, University of California at Berkeley, Berkeley, CA 94720, USA.

^cDepartment of Chemistry, University of California at Berkeley, Berkeley, CA 94720, USA.

^dSchool of Public Health, University of California at Berkeley, Berkeley, CA 94720, USA.

475

*Yutong Liang or Allen H. Goldstein

Email: yutong.liang@berkeley.edu or ahg@berkeley.edu.

480

This PDF file includes:

Supplementary text

Figures S1 to S18

485 Tables S1 to S5

SI References

490

Extended Materials and Methods

Data Sources and Study Regions. The PurpleAir sensors report the mass of size-resolved particulate matter, as well as environmental parameters such as temperature and relative humidity (RH). Data from many of these sensors are voluntarily shared online by the owners (including the citizens, and government agencies like the California Air Resources Board, Bay Area Air Quality Management District and Southern California Air Resource Board). For this study we downloaded the 10-min average $PM_{2.5}$ concentration data from the PurpleAir website (<https://www2.purpleair.com/>). For the NC 2020 case, we used data from the areas boxed by latitudes [38.77° N, 38.04° N] and longitudes [123.19° W, 121.15° W]; [38.04° N, 37.98° N] and [123.19° W, 121.60° W]; [37.98° N, 37.67° N] and [122.69° W, 121.90° W]; [37.67° N, 37.21° N] and [122.47° W, 121.36° W] for August and September 2020 (Fig. S2). These boxes cover most of the San Francisco Bay Area and part of the Sacramento County. In this period, residents in this area experienced smoky days caused by the LNU Lightning Complex Fire, the August Complex Fire, the SCU Lightning Complex Fires, the CZU Lightning Complex Fires, and at the end of September the Glass Fire, as well as the massive fires in Oregon (<https://www.fire.ca.gov/incidents/2020/>). The same study area was used in the NC 2018 case, although fewer sensors were operating at that time. The study area for the SC 2020 case is boxed by [33.47° N, 34.50° N] and [116.85° W, 119.40° W], as shown in Fig. S3.

Selection of Sensor Correction Models. Plantower sensors (Plantower Technology) used by PurpleAir measure the mass of particulate matter by measuring light scattering at 680 ± 10 nm (1). The manufacturer has a proprietary algorithm to convert the light scattering signal to the mass concentration of particulate matter. Each sensor is also embedded with a BME 280 sensor (Bosch Sensortec) to measure the temperature, pressure, and relative humidity in real time. The performance of low-cost $PM_{2.5}$ sensors is dependent on humidity, temperature and level of particulate matters (2–7). Many corrections have been proposed to convert the raw $PM_{2.5}$ data ($PM_{2.5} CF=1$) measured by Plantower sensors to values consistent with research grade instruments. In our analysis, hourly average primary $PM_{2.5}$ data measured by 16 EPA Air Quality Measurement Stations (AQMSs) in August and September 2020 in the study area was downloaded from the EPA AirNow's API website (<https://docs.airnowapi.org/>). According to the California Air Resource Board (<https://ww2.arb.ca.gov/our-work/programs/ambient-air-monitoring-regulatory/annual->

[monitoring-network-report](#)), the primary $PM_{2.5}$ monitors in these sites are MetOne BAM (beta-ray attenuation) continuous monitors. For each EPA measurement site, we compared the data measured by outdoor PurpleAir sensors within 5 km (using at most 50 sensors near each EPA site to avoid data being skewed towards a small number of sites). We excluded outdoor sensors that (a) reporting less than 4 weeks of data. (b) had weak correlation with the EPA station's measurement ($r < 0.8$) because it might be affected by other local pollution sources or it could be listed as an outdoor sensor by mistake, (c) reported $PM_{2.5}$ larger than $800 \mu g m^{-3}$ and sensors always reporting data lower than $10 \mu g m^{-3}$ as they were either malfunctioning or were operating outside of the recommended limits of detection. In total, data from 446 outdoor sensors surrounding the 16 EPA sites were included in the correction factor evaluation.

To get correction factors for converting PurpleAir sensor measurements to federal reference/equivalent method measurements, some studies performed a linear regression of $PM_{2.5}$ measured by the PurpleAir sensors with data from nearby EPA regulatory instruments (2), while others also considered the effect of temperature and relative humidity on the sensor's performance (5, 8, 9). There are two main types of PurpleAir sensors available for purchase on the PurpleAir website (<https://www2.purpleair.com/collections/air-quality-sensors>). The PA-I sensors only have one channel (Plantower PMS 1003) for PM measurement. Each PA-II PurpleAir sensor has two Plantower PMS 5003 sensors inside (Channel A and Channel B). Ideally, it is good to average the values reported by the two sensors and to remove some abnormal data because of sensor failures that can be captured by the difference of PM reported for the two channels. However, many sensors did not report $PM_{2.5}$ data from Channel B, presumably because they were the indoor PA-I sensor model. To incorporate as many sensors (buildings) as possible in the analysis, we only used Channel A data if data from both channels are available. According to the evaluation by Barkjohn et al. (8), the $PM_{2.5}$ concentrations reported by Channels A and B agree well. In line with this prior result, we compared 42 sensors with fully available Channel A and B data and found excellent agreement [slopes of linear fit between two channels' $PM_{2.5}$ data have IQR of (0.97, 1.06) with median at 1.01; R^2 of fit between two channels' $PM_{2.5}$ are all above 0.95]. More broadly, we believe that many instances of abnormal data are reliably excluded by our other QA/QC procedures (described in "Other QA and QC" section below). The sensors report both $PM_{2.5} CF = 1$ data and $PM_{2.5} CF = ATM$ (atmospheric) data. It is not known how the $CF = 1$ data are converted to $CF = ATM$ data in the

proprietary algorithm from the manufacturer. However, it is known that the ATM data can result in a nonlinearity for concentrations below and above around 20-40 $\mu\text{g m}^{-3}$ (10, 11), while CF = 1 data do not have this problem. The PM_{2.5} CF = 1 data have also been shown to correlate better with the EPA federal reference methods or federal equivalent methods. The PM_{2.5} CF = 1 data were therefore chosen as the raw input data in our calibration.

Seven correction methods were compared in our analysis, with their performance summarized in Table S1. Method 1 and 2 are based on linear regressions (ordinary least square method) of the EPA PM_{2.5} data with the PurpleAir PM_{2.5} CF = 1 data (of individual sensors, not the average of all sensors within 5 km of each AQMS). Method 3 uses an orthogonal distance regression (ODR) with zero intercept. The Barkjohn *et al.* (9) US fire correction was based on comparison of PurpleAir measurement data with collocated federal equivalent methods in 7 sites across the United States affected by prescribed fires, ambient aged fires, woodstove fires and wildfires. It considers the effect of relative humidity on the measurement. A similar field comparison was performed by Holder *et al.* (3). The correction factors from these two studies were also evaluated here for our dataset. We also constructed a “New fit incorporating RH” correction by a multivariate regression of EPA PM_{2.5} against PM_{2.5} and RH measured by nearby outdoor PurpleAir sensors using data in August and September 2020 from the San Francisco Bay Area. In some studies, a nonlinear RH term $\text{RH}^2/(1-\text{RH})$ was used (5, 8). However, recently it has been demonstrated that a linear term of RH can perform even better than the non-linear term (6). Therefore, the linear RH function is used in our “New fit incorporating RH” correction. Finally, using EPA PM_{2.5} as the response, and PM_{2.5} and RH reported by the nearby PurpleAir sensors as input, we trained a binary decision tree for regression model using the Statistics and Machine Learning Toolbox in MATLAB. The temperature term was not included in our correction models because it has been shown that including the temperature term can only negligibly improve the performance of such correction models (5, 6). The commonly used Lane Regional Air Protection Agency (LRAPA) correction, which uses the CF = ATM data in the correction equation (6), was not compared here.

Adding a non-zero intercept to the model did not substantially improve the R^2 or reduce the root mean square error (RMSE). A major disadvantage of adding such an intercept is it can lead to an overestimation when the PM_{2.5} concentration is very low. We also evaluated whether the linear regression

of the EPA PM_{2.5} data with the PurpleAir PM_{2.5} (CF = 1) data are sensitive to the distance threshold. Table S2 shows that the regression coefficients are not very sensitive to the distance threshold from 2 km to 20 km.

In ordinary least square regression, it is assumed that the independent variable is free from errors (13). However, this assumption may not be true for PurpleAir sensor measurements. We therefore also calculated the slope using orthogonal distance regression (ODR). The ODR minimizes the sum of orthogonal distances of the data points from the regression line (13). Using the ODR method changed the correction factor by only 0.01 and increased the RMSE (Table S1). Adding RH in the linear regression also only made an almost negligible improvement. We therefore chose the linear regression without intercept correction. In this case, the fitted correction factor is 0.53. Fig. S6 displays the hourly concentration time profiles of PM_{2.5} measured by each EPA monitor in the San Francisco Bay Area, and the average concentrations of PurpleAir sensors (after correction with CF = 0.53) within 5 km in August and September 2020. They agree reasonably well with each other.

It is important to note that the correction equations evaluated here are only applicable for this analysis, and they should not be generalized to other places and/or at other times. As shown in Holder *et al.* (3), even the correction factors for wildfire smoke from different fires in the US can differ by a factor of more than 2. It is also worth noting that our analysis is not heavily dependent on the exact correction factor because the concentration ratios are the targets. The correction factors only affected which peaks were defined as indoor source peaks. When wildfire smoke affected a region, the composition of indoor and outdoor PM_{2.5} were expected to be similar because wildfire particles dominated even in the indoor environments (Table 1). Therefore, it is reasonable to use the same correction for both indoor and outdoor PM_{2.5}, especially we focus on the indoor/outdoor ratios, as suggested by Bi *et al.* (14).

As shown in Table S1 and Fig. S15, the binary decision tree method can improve the correlation of PurpleAir data with EPA measurements. Results from the same analysis with this correction are shown in Fig. S16. The trend of the result is the same as the no-correction case, but the difference between the fire days and non-fire days are larger, which is probably due to a non-zero intercept in the correction.

We also performed regression for the correction of Greater Los Angeles Area sensors (SC 2020 case). Based on linear regression of EPA monitor data with the nearby PurpleAir sensor using the same

approach as in the NC 2020 case, a correction factor of $\beta_1 = 0.58$ was adopted (NRMSE = 0.42, see Figures S8-S9). Similar analysis has been performed by Delp and Singer (2) for San Francisco Bay Area sensors in November 2018. A correction factor of $\beta_1 = 0.48$ was adopted in our analysis.

Other QA and QC. We selected indoor sensors that had measurement value for at least 1/6 of the time (~10 days) in the two-month period considered in our study. We found 1459 indoor monitors in this region meeting this criterion. For each indoor sensor selected, we used its longitude and latitude to locate the nearest outdoor sensor. More than 2000 outdoor sensors in this region reported at least 10 days data during the period considered, compared with only 16 EPA Air Quality Monitoring Stations (AQMS) in this region. The geometric mean (GM) distance from an indoor sensor to the nearest AQMS is 6.7 km, but it is only 0.21 km to the nearest outdoor sensor (Fig. S17). The substantially reduced distance allows much more accurate evaluation of indoor/outdoor concentration relationships. To prevent the possibility that the nearest outdoor sensor was located near major pollution sources, when the nearest outdoor sensor is more than 500 m away from the indoor sensor, we required the 50th percentile concentration at this outdoor node when it was not affected by wildfires to be below $25 \mu\text{g m}^{-3}$, according to the levels and spatial decay rate of $\text{PM}_{2.5}$ measured near roads (15–18). We further required the outdoor sensor to cover at least 85% of the time when the indoor sensor reported data. If the $\text{PM}_{2.5}$ concentration measured by an “indoor” sensor is correlating too well with a nearby outdoor sensor ($r^2 > 0.8$), it is likely that this sensor was placed outdoors. This mislabeled or dislocated sensor is therefore not used in the analysis. Fig. S18 shows an example of an indoor node discarded for this reason. We removed 165 “indoor” sensors from the analysis because of this problem. Another 20 indoor sensors were not considered because we could not find a nearby outdoor sensor that reported data for more than 85% of the time when the indoor sensor reported data. With all these criteria in place, data from $N = 1274$ indoor sensors in this region could be used. The same procedure was applied to data in the NC 2018 and SC 2020 cases. Negative values of $\text{PM}_{2.5}$ concentration were also discarded.

Decomposition of Indoor $\text{PM}_{2.5}$ We separated the indoor $\text{PM}_{2.5}$ from indoor and outdoor origins by removing short-term indoor $\text{PM}_{2.5}$ peaks that were unlikely due to penetration. A very similar approach has

been demonstrated in previous studies by Allen *et al.* (19, 20). According to high time-resolution measurements of particulate matter in previous indoor studies, the major indoor emission processes (mainly cooking and cleaning) typically last for half an hour to an hour, and after that a longer period is needed for the PM_{2.5} perturbation to decay to less than half of its peak value (21). When these processes happen, the indoor level of PM_{2.5} was at least 30 µg m⁻³. We therefore selected all the peaks with half-prominence width (w) between 1 hour and 4 hour and prominence level above 30 µg m⁻³ as indoor-source peaks. It is possible that in some buildings the windows were opened for around an hour during the fires and created peaks that meet this criterion. Out of the 1274 buildings considered, we identified these large indoor source peaks in 834 buildings. Buildings without such peaks might be commercial buildings without large indoor PM_{2.5} sources, or the sensor in that building was placed in a location free from large indoor emissions. We assumed the indoor PM_{2.5} other than that caused by these large peaks to be infiltrated PM_{2.5}. We reconstructed the infiltrated PM_{2.5} by linearly interpolating indoor PM_{2.5} concentration 3w before and after these large peaks with respect to time. The long 3w window was chosen to ensure that the indoor source peaks can be more thoroughly removed. For data outside of this window, the indoor concentration was assumed to be equal to the infiltrated PM_{2.5}. As a QA/QC step, if the calculated non-cooking indoor concentration was higher than outdoor concentration, that data point was removed from the analysis.

Mass Balance Model and Total Indoor Particle Loss Rate Constant Calculation. The indoor concentration of PM_{2.5} depends on infiltration, indoor emission, and loss. We explored the dynamics of indoor PM_{2.5} with a box model. If we assume the PM_{2.5} is well-mixed indoors, the mass balance of PM_{2.5} in a building can be written as:

$$V \frac{dC_{in}}{dt} = aPVC_{out} - aVC_{in} - k_{loss}VC_{in} + S \quad (S1)$$

where V is the volume of the room, a is the air exchange rate, P is the penetration factor of particles, k_{loss} is the loss rate constant including deposition and indoor filtration, and S is the indoor emission rate. C_{in} and C_{out} are the indoor and outdoor concentrations, respectively (22, 23). Dividing by V on both sides, we can simplify the equation to:

$$\frac{dC_{in}}{dt} = aPC_{out} - (a + k_{loss})C_{in} + \frac{S}{V} \quad (S2)$$

When the indoor and outdoor particles are in steady state, and S is small, we have:

$$\frac{dC_{in}}{dt} = 0 = aPC_{out} - (a + k_{loss})C_{in} \Rightarrow F_{in} = \frac{C_{in}}{C_{out}} = \frac{aP}{a + k_{loss}} \quad (S3)$$

where F_{in} is the infiltration factor. For particulate matter, F_{in} can be obtained from the ratio of indoor/outdoor concentration when there are no outdoor sources (23, 24). Another way to estimate F_{in} is to regress the indoor $PM_{2.5}$ on outdoor values (25). However, this method has been shown to underestimate the infiltration factor while overestimating the indoor background (23), or produce infiltration factors outside [0,1] (14). Therefore, the ratio method was used for our analysis.

During the peak of cooking-like indoor particle release events, the indoor $PM_{2.5}$ resulting from cooking is much larger than the infiltrated smoke. When the indoor emission event is over, we assume the indoor source term becomes 0, and we have:

$$\frac{dC_{in}}{dt} = -(a + k_{loss})C_{in} \Rightarrow C_{in}(t - t_{peak}) = C_{in,peak} e^{-(a+k_{loss})(t-t_{peak})} \quad (S4)$$

Therefore, $(a+k_{loss})$ can be estimated by fitting the curve of $C_{in}(t)$ (26). We define $(a+k_{loss})$ as the total indoor particle loss rate constant (λ_t). A peak prominence of $30 \mu g m^{-3}$ ($20 \mu g m^{-3}$ in the SC 2020 case to incorporate more peaks) was used as the threshold to find large indoor peaks that were subsequently used in the particle loss rate constant calculation. If windows were opened and then closed, the decay of resulted indoor $PM_{2.5}$ can also be described by Equation S4. Those peaks were also included because the decrease of indoor $PM_{2.5}$ under that circumstance can also be described by the exponential decay. The decay rate constant is also not substantially affected by the correction factor used because the correction factor affects C_{in} and $C_{in, peak}$ in the same way. To get total particle loss rate $\lambda_t = a+k_{loss}$, Equation S4 can be rewritten as:

$$-\ln \frac{C_{in}(t)}{C_{in}(t_{peak})} = \lambda_t(t - t_{peak}) \quad (S5)$$

We then linearly fitted this equation by least square method to get slope λ_t for the decay of each peak of indoor $PM_{2.5}$. In this part, we no longer require the width of the peak to be above 1 hour. In this way, indoor $PM_{2.5}$ peaks resulting from short-time window opening were also used to get λ_t . The 95% confidence

interval of λ_t was also calculated. To ensure the exponential decay model is applicable, if the lower bound of the confidence interval of λ_t for a peak was below zero, this peak was not used as data for Fig. 5.

The decrease of indoor PM_{2.5} concentration can also be caused by the decrease of outdoor PM_{2.5} concentration. In such cases, the assumption that incoming outdoor PM_{2.5} source is stable no longer holds. Therefore, if the indoor PM_{2.5} was decaying together with the outdoor PM_{2.5} measured by the nearest sensor ($r^2 > 0.8$), this peak was excluded from the analysis. For the 1274 buildings considered in the NC 2020 case, we observed such decay peaks in 1000 buildings. On average, 4.7 decay peaks were captured in each building in the two-month period.

Uncertainty of the infiltration ratios and the decay rate constants

We roughly estimated the uncertainty of the infiltration ratios of individual sensor pairs, based on the idea that disagreement among any two paired sensors would lead to an uncertain estimate of the ratio of concentrations between those sensors. Thus, we gain a magnitude estimate of the uncertainty of the indoor/outdoor concentration ratio by examining the disagreement among a large number of paired nearby *outdoor* sensors across the PurpleAir dataset in our domain. We consider two timescales: (1) the uncertainty of the indoor/outdoor ratios of the 10-min data, reflecting the transient noise at short time scales, and (2) the uncertainty of the infiltration ratio for a building over the two-month period in the analysis, reflecting the possible range of persistent-sensor-to-sensor bias. To do so, we first found the outdoor sensors that were used to calculate indoor/outdoor ratios. Since it is possible that the nearest outdoor sensor of multiple indoor sensors is the same sensor, for the 1274 pairs of sensors, there are only 784 outdoor sensors used. For each sensor, we tried to find the nearest outdoor sensor within 1 km, which was successful for 775 sensors. For each pair of sensors i at time j , we calculate the ratios of $x_{i,j}/y_{i,j}$, where $x_{i,j}$ is the concentration of the i^{th} of the 775 used outdoor sensors at time t , and $y_{i,j}$ is the concentration of its nearest outdoor sensor. We make \mathbf{R}_i as:

$$\mathbf{R}_i = \left[\frac{x_{i,1}}{y_{i,1}}, \frac{x_{i,2}}{y_{i,2}}, \dots, \frac{x_{i,n}}{y_{i,n}} \right]^T \quad (\text{S6})$$

Then we concatenate the \mathbf{R}_i array into \mathbf{R}_{all} array by:

$$\mathbf{R}_{all} = [\mathbf{R}_1 \mathbf{R}_2 \dots \mathbf{R}_n]^T \quad (S7)$$

The uncertainty of the indoor/outdoor ratio of 10-minute data is reflected by the variation of \mathbf{R}_{all} , which yields 0.886, 1.005, and 1.138 as 25th, 50th, and 75th percentiles values, respectively.

710 The uncertainty of the infiltration ratio for a building over the two-month period can be roughly estimated by the statistics of $median(\mathbf{R}_i)$, which has 0.955, 1.035, and 1.131 as 25th, 50th, and 75th percentiles values, respectively. Therefore, we can conclude that the uncertainty of the infiltration ratio for a building over the two-month period is less than $\pm 10\%$.

715 The decay rate calculation should have a very small uncertainty due to any bias in PA sensors because it uses measurements only from a single indoor sensor. We were fitting the decay curves of individual sensors by:

$$-\ln \frac{C_{in}(t)}{C_{in}(t_{peak})} = \lambda_t (t - t_{peak}) \quad (S5)$$

in which $C_{in}(t)$ ratios by the same sensor (especially in the same peak) should have very small uncertainty.

720 Given the reasons stated above, we expect the exposure reduction calculations have even lower uncertainties because we are averaging the exposure reduction of the 1274 buildings. Assume uncertainty of the infiltration ratio for a building over the two-month period is 10%, the average of infiltration ratios of all the buildings will have an uncertainty of $10\% / \sqrt{1274} = 0.28\%$ following central limit theorem. More conservatively, the median uncertainty of the infiltration ratio over two months, as reported for 774 sensor pairs above, was 1.035, or 3.5%. In either case, this uncertainty is quite small. We expect that the average exposure reduction would have a quantified uncertainty of similar or better magnitude to the I/O ratio, in 725 other words, well less than 5%. Other unquantifiable uncertainties – e.g., differential or non-linear response of the PurpleAir to time-varying aerosol properties – add additional uncertainties that are more difficult to directly estimate, but we believe that these uncertainties do not fundamentally undermine the validity of our qualitative results.

730 **Building information.** Property data for PurpleAir Indoor-Outdoor comparison analysis were obtained by matching coordinates to addresses, verifying the addresses, looking up the addresses on publicly available property listing services, and finally quality control of the resulting data. The latitude-longitude coordinates were obtained from the publicly available PurpleAir database formally from a PurpleAir JSON file (purpleair.com/json – defunct as of December 2020), now available through the official PurpleAir API (api.purpleair.com). The coordinates contain 6 decimal places of precision and thus are accurate to under 10 meters, however, the placement is based on the available WiFi signal and can be edited by the sensor owner to be located anywhere on the map. As such, there is some uncertainty introduced into the reverse geocoding process, but since citizen scientists are interested in air quality within their own homes and research groups require spatial fidelity it can be assumed these coordinates are approximately correct.

740 After obtaining the list of coordinates, the Google and ArcGIS geocoding engines performed reverse geocoding scripted using the Python library OSMnx 1.0.1 (osmnx.readthedocs.io/en/stable/). About 38.5% of addresses in the SF Bay region disagreed between Google and ArcGIS lookups. The reasons for the disagreements are due to placement in homes leading to low confidence assigning addresses to lots such as on a street corner. The sensor labels and manual searches on Google Maps were used to confirm 745 the address. If the sensor label contains the address or a partial address or is obvious from the Google Map manual search, the confidence to the matched address is high. If the reverse geocoded searches match, then the confidence is medium, otherwise, it is assigned low confidence. From this analysis of valid address (n=1274), 13% were assigned high confidence, 73% were assigned medium confidence, and 14% were assigned low confidence. For low confidence addresses, the ArcGIS address was used.

750 The list of addresses was then manually inputted to Zillow, a publicly accessible website which offers data on homes and apartments using multiple listing services and county databases including building age, HVAC information, and livable area. Zillow furthermore uses existing publicly available information as well as a proprietary algorithm to derive an estimate of the current (as of December 2020) evaluation of the home or apartment (rent if a rental unit) termed a “Zestimate®.” If the address matches an 755 apartment complex, the first listed unit was then used to find the year of construction, HVAC information,

and a bell-weather of the typical price and area of apartments since these can vary within complexes. From the 1274 address, 79.5% returned the year of construction, 83.6% returned HVAC data, 76.7% returned a price estimate, and 72.2% returned the area. Out of the 1274 buildings analyzed, 1112 (87%) buildings were found to be residential. Among these residential buildings, 80%, 13%, and 4% were matched to single-family houses, condominiums or multi-family buildings, and apartments, respectively.

As an additional sensitivity analysis, we restricted our dataset to the 87% of buildings that could unambiguously be ascertained to be residential. For this restricted dataset, the mean infiltration ratios on both fire days and non-fire days changed by less than 0.01.

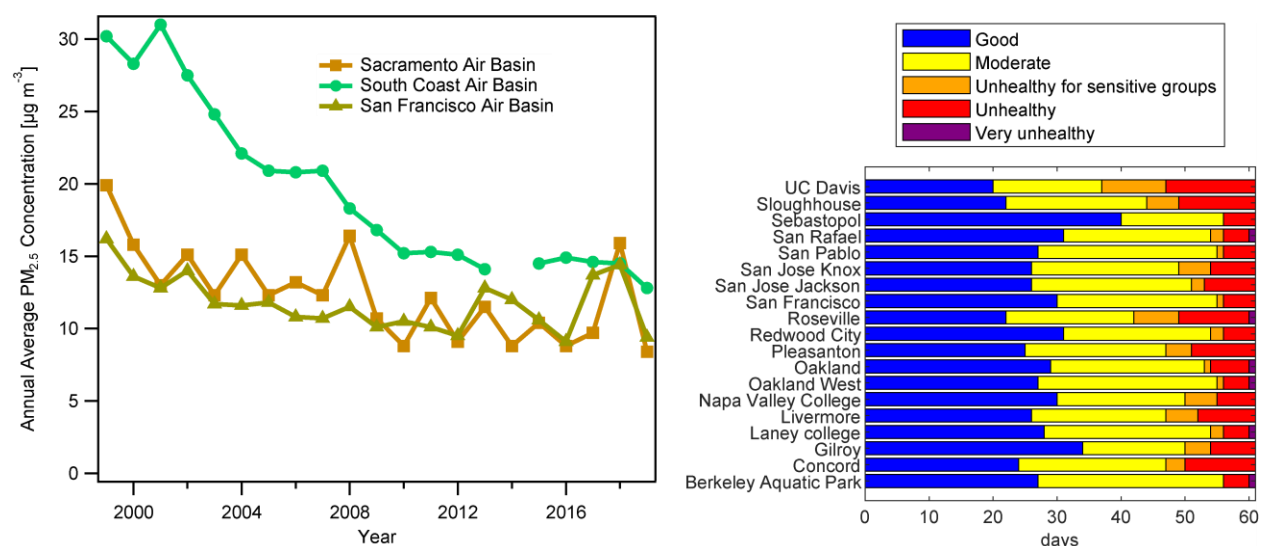
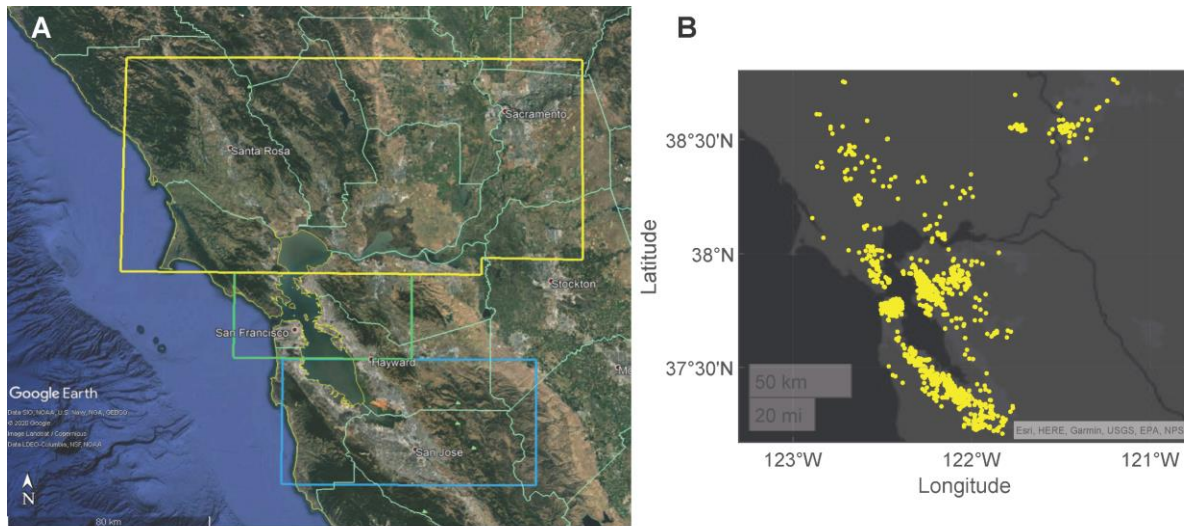
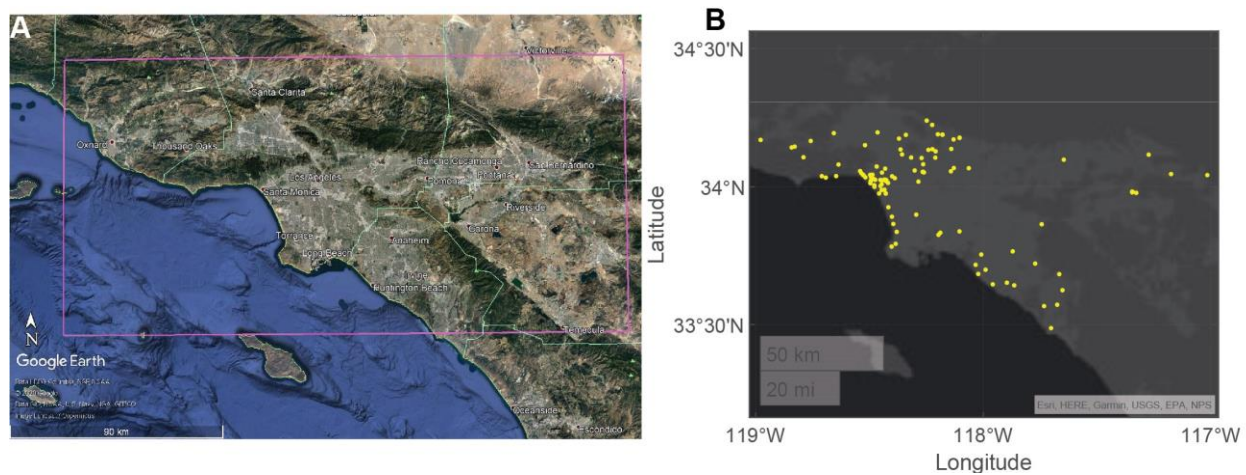


Fig. S1. A. Annual average PM_{2.5} concentrations in 3 Air Basins in California from 1999 to 2019 (Data retrieved from California Air Resource Board website <https://www.arb.ca.gov/adam>). The missing point is because of insufficient data available to determine the value. **B.** San Francisco Bay Area Air Quality Index (AQI) category in August and September 2020 based on 24-hour average level of PM_{2.5} at each EPA Air Quality Measurement Station. 0 - 15.4 µg/m³: Good; 15.5 - 35.4 µg/m³: Moderate; 35.5 - 55.4 µg/m³: Unhealthy for sensitive groups; 55.5 - 150.4 µg/m³: Unhealthy; 150.5 - 250.4 µg/m³: Very unhealthy.



775 **Fig. S2. A.** Study regions in the San Francisco Bay Area. Google Earth imagery © 2020 Google. PurpleAir
sensors in the three boxes were analyzed together. **B.** Locations of all the indoor PurpleAir sensors included
in the NC 2020 case.



780 **Fig. S3. A.** Study region in the Greater Los Angeles Area. Google Earth imagery © 2020 Google. **B.** Locations of all the indoor PurpleAir sensors included in the SC 2020 case.

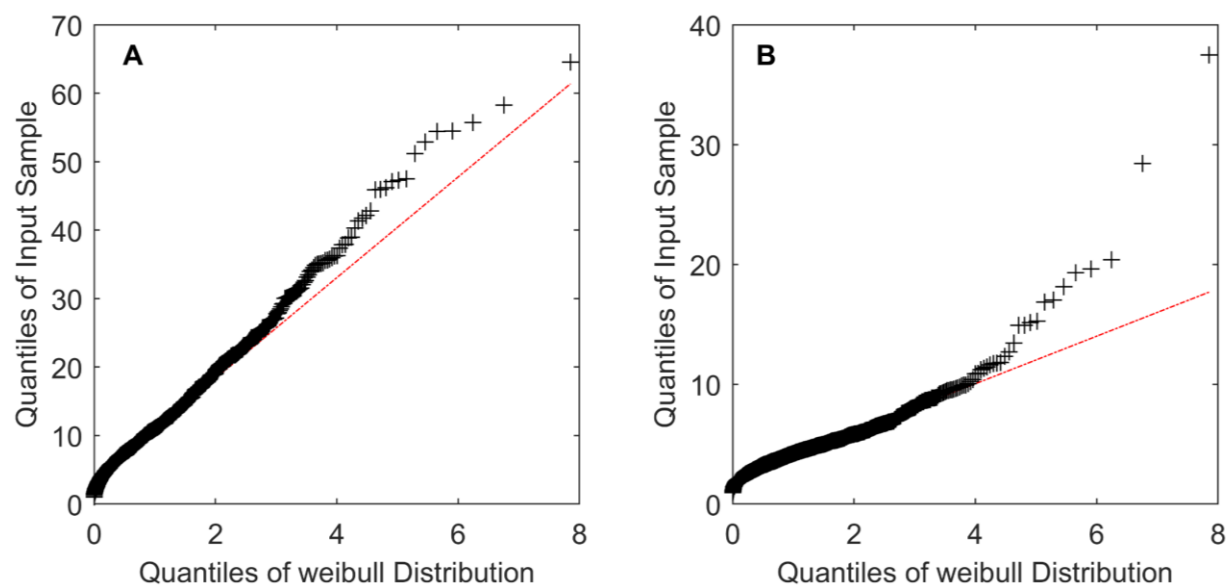


Fig. S4. Quantile-quantile plots of mean indoor $\text{PM}_{2.5}$, on the fire days **(A)** and non-fire days **(B)** against Weibull distribution. The reference line represents the theoretical Weibull distribution.

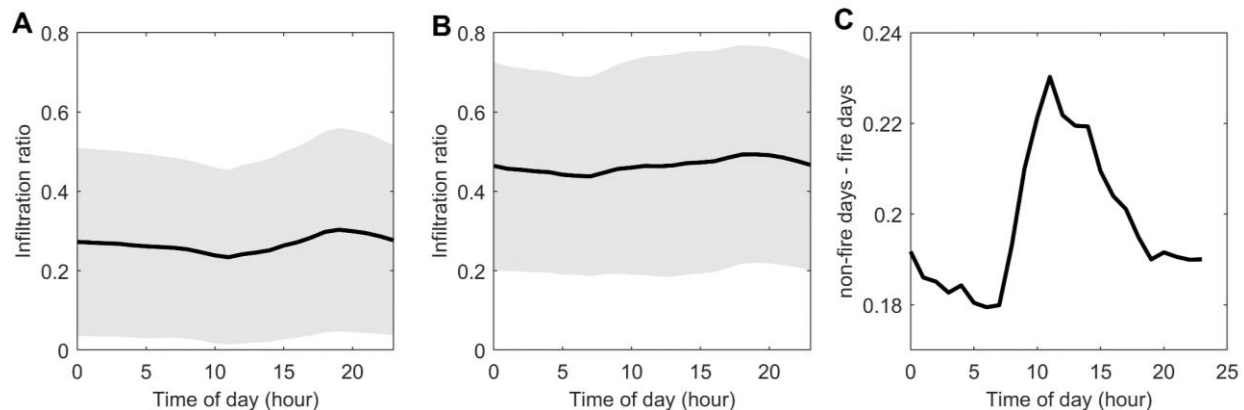


Fig. S5. Diel plots (local time) **A.** Infiltrated $PM_{2.5}$ /outdoor $PM_{2.5}$ on fire days and **B.** Infiltrated $PM_{2.5}$ / outdoor $PM_{2.5}$ on non-fire days **C.** Diel plot of the difference in infiltrated $PM_{2.5}$ / outdoor $PM_{2.5}$ (non-fire days – fire days). Gray shading in A & B shows the standard deviation. Data are average of all the PurpleAir sensors in the NC 2020 case. The difference in mean infiltration ratio between fire days and non-fire days are most apparent in the daytime, consistent with more ventilation typically occurring during daytime.

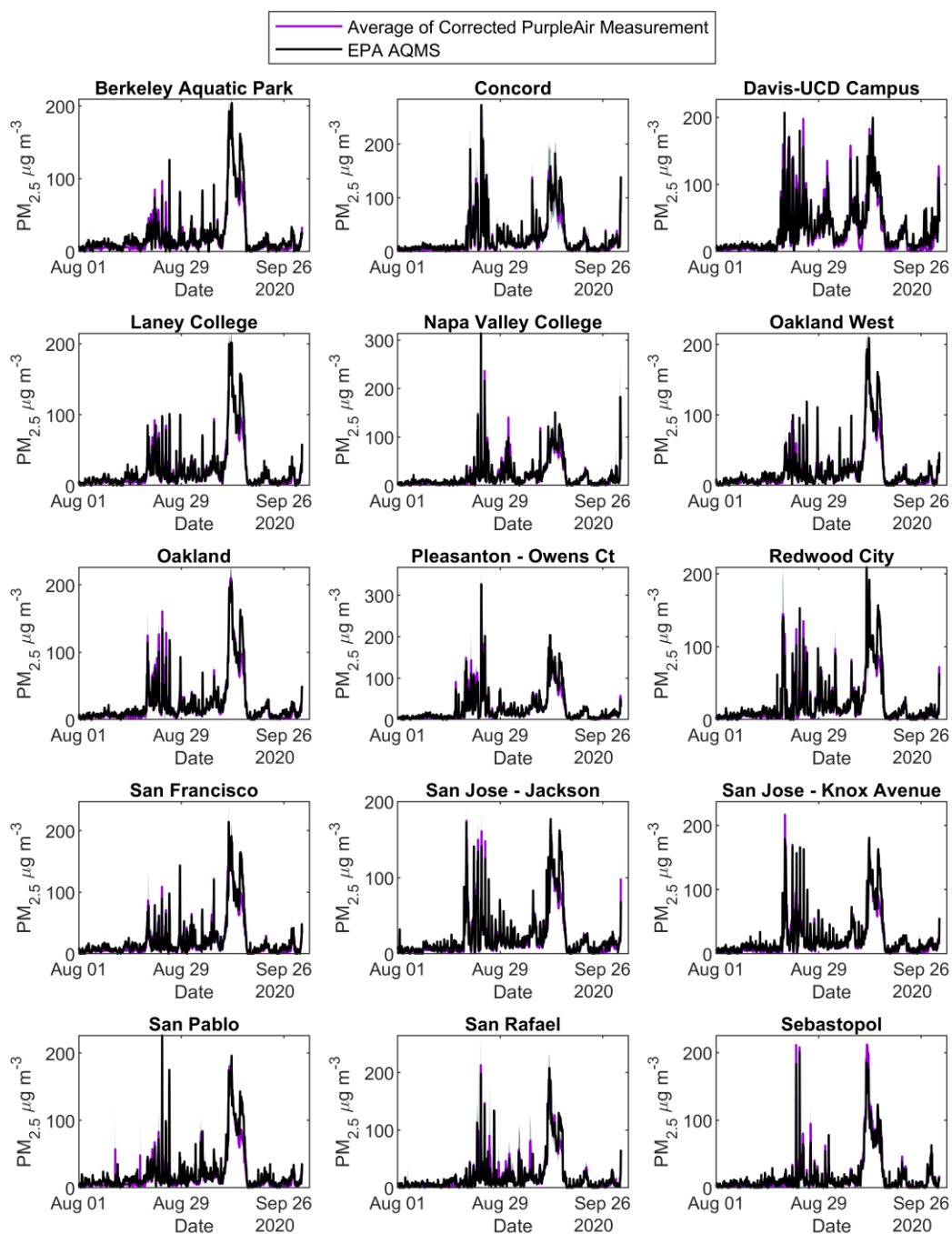


Fig. S6. Hourly time profile of $PM_{2.5}$ concentration of the EPA monitors (black) and mean (purple) \pm standard deviation (gray) of $PM_{2.5}$ (corrected) measured by nearby PurpleAir sensors in the San Francisco Bay Area in August and September 2020. The plots only include EPA monitoring stations having at least three

outdoor PurpleAir sensors within 5 km of them. The EPA measurement and nearby PurpleAir sensors
 800 measurement agree reasonably well with each other.

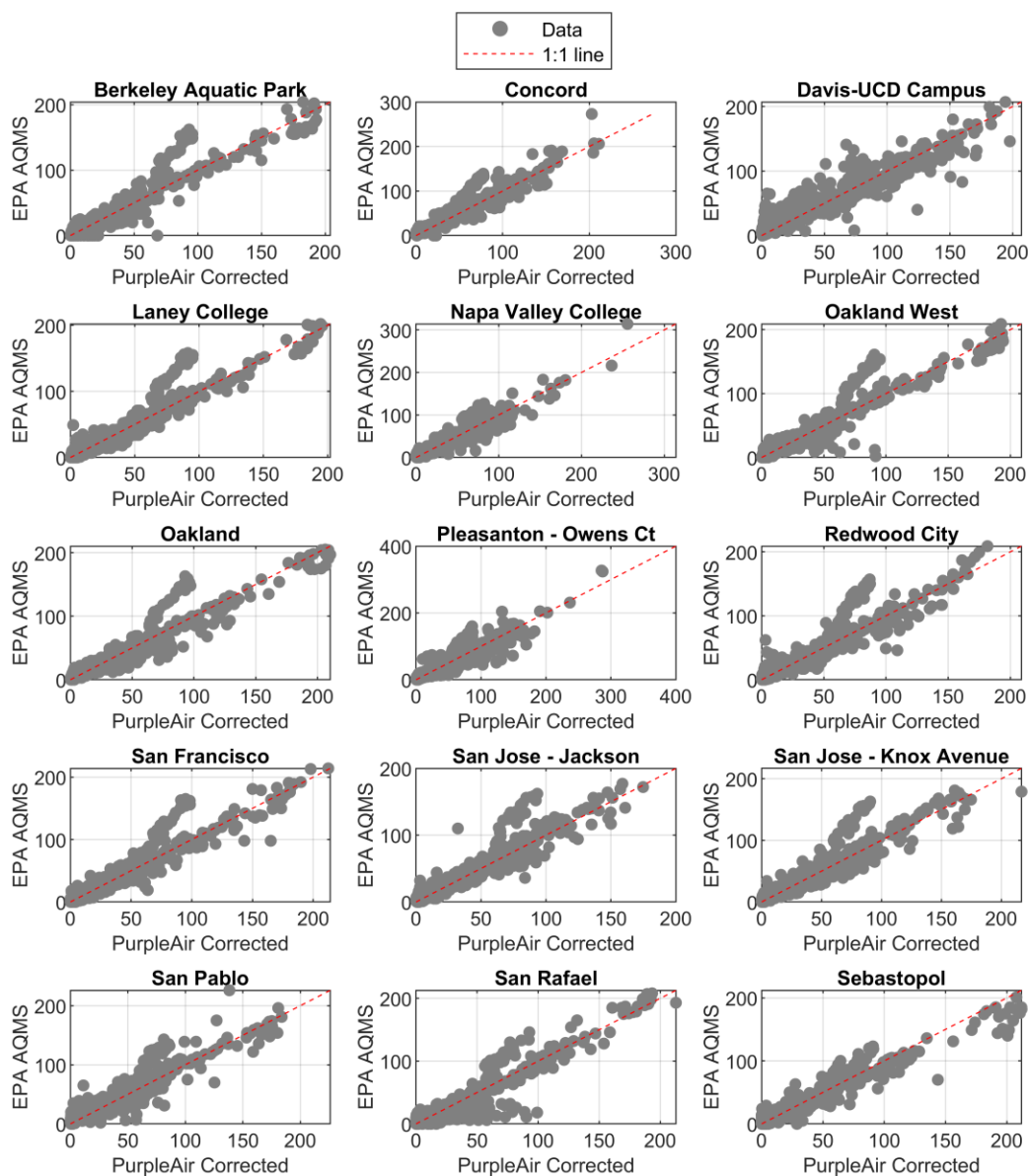


Fig. S7. Scatter plot of $\text{PM}_{2.5}$ ($\mu\text{g m}^{-3}$) of the EPA monitors and mean $\text{PM}_{2.5}$ (corrected) measured by nearby PurpleAir sensors in the San Francisco Bay Area in August and September 2020.

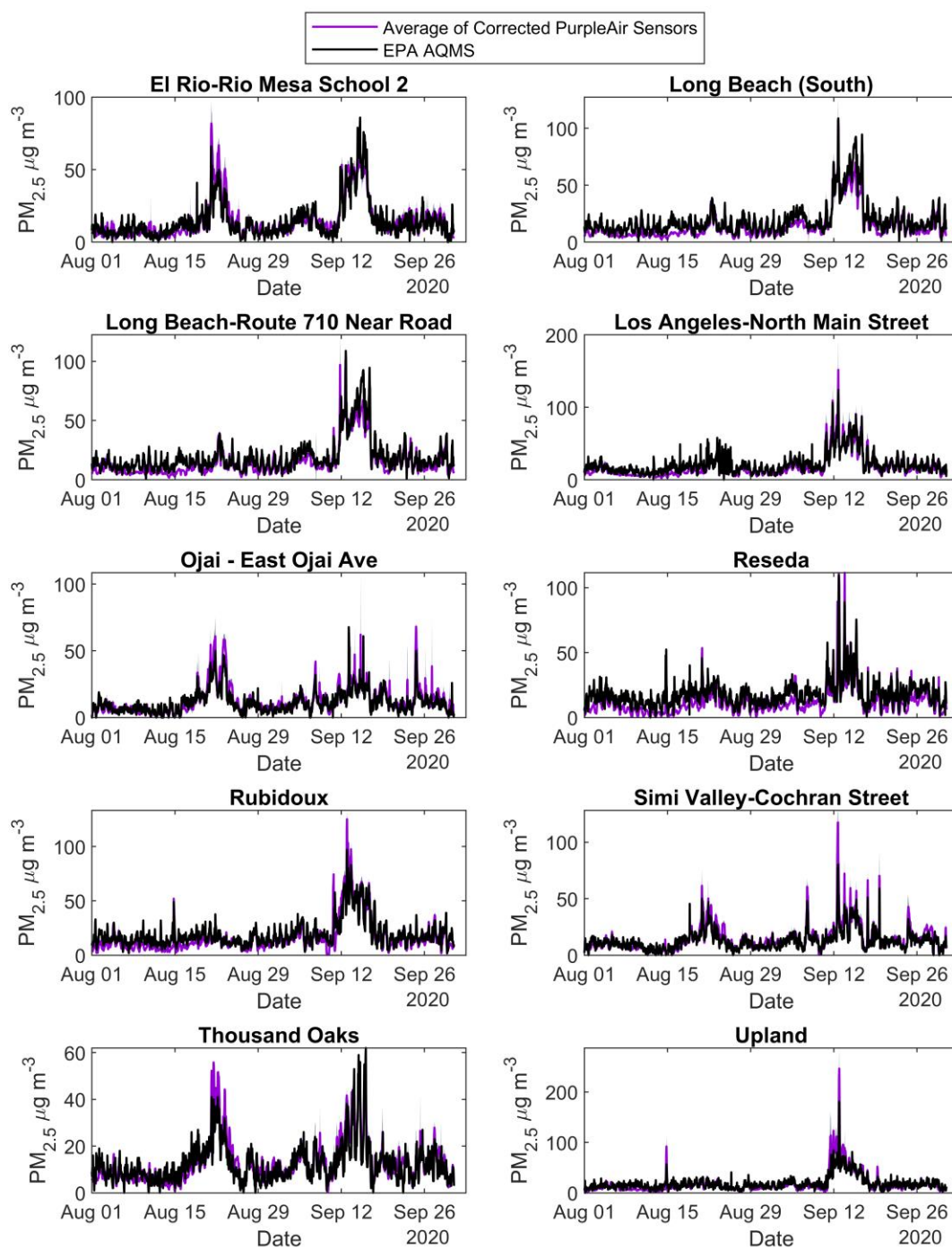


Fig. S8. Hourly time profile of $PM_{2.5}$ concentration of the EPA monitors and mean (purple) \pm standard deviation (gray) of $PM_{2.5}$ (corrected) measured by nearby PurpleAir sensors in the Greater Los Angeles Area in August and September 2020. The plots only include EPA monitoring stations having at least three outdoor PurpleAir sensors within 5 km of them.

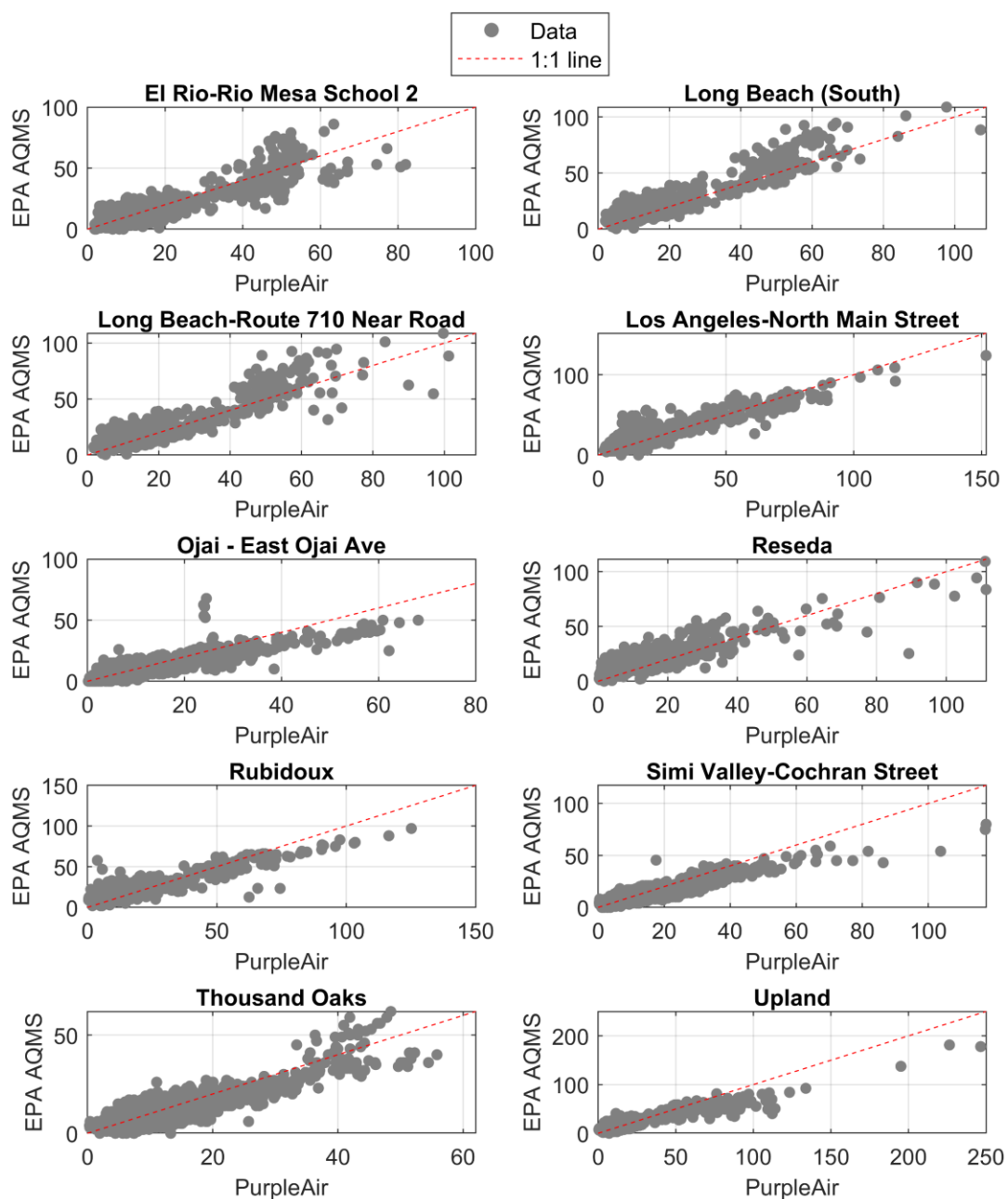


Fig. S9. Scatter plot of $\text{PM}_{2.5}$ ($\mu\text{g m}^{-3}$) of the EPA monitors and $\text{PM}_{2.5}$ (corrected) measured by nearby PurpleAir sensors in the Greater Los Angeles Area in August and September 2020

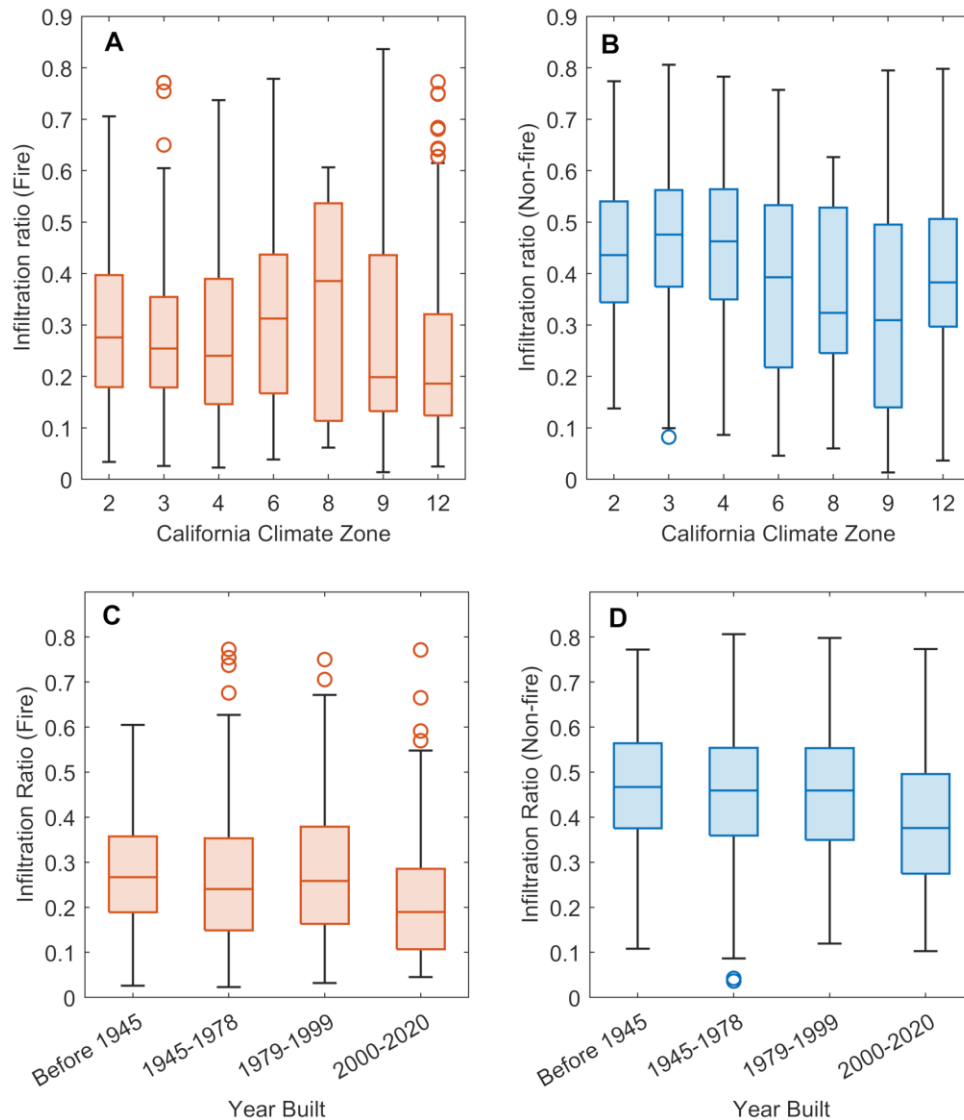


Fig. S10. Infiltration ratio of buildings in different climate zones **A.** on fire days (ANOVA $p = 0.004$); **B.** non-fire days (ANOVA $p < 10^{-3}$) in August and September 2020. Only climate zones with at least 10 indoor sensors being analyzed are included in this figure. Reference cities for different climate zones (which were included in our study) are: Zone 2-Napa, Zone 3-San Francisco & Oakland, Zone 4-San Jose, Zone 6-Los Angeles (LAX), Zone 8-Long Beach, Zone 9-Los Angeles (Civic Center), Zone 12-Sacramento (27). Infiltration ratio of residential buildings (NC 2020 case) built in different periods **C.** on fire days (ANOVA $p = 0.004$); and **D.** on non-fire days (ANOVA $p < 10^{-3}$). Only residential buildings are considered in C and D. Buildings in Zone 12 had lower infiltration ratios than other Northern California climate zones considered.

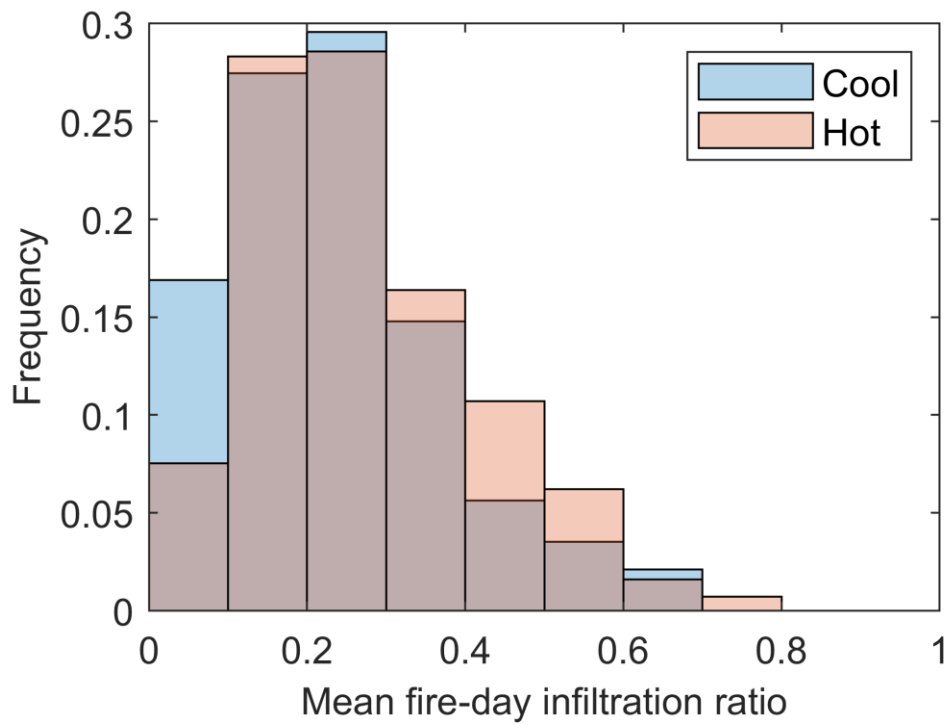
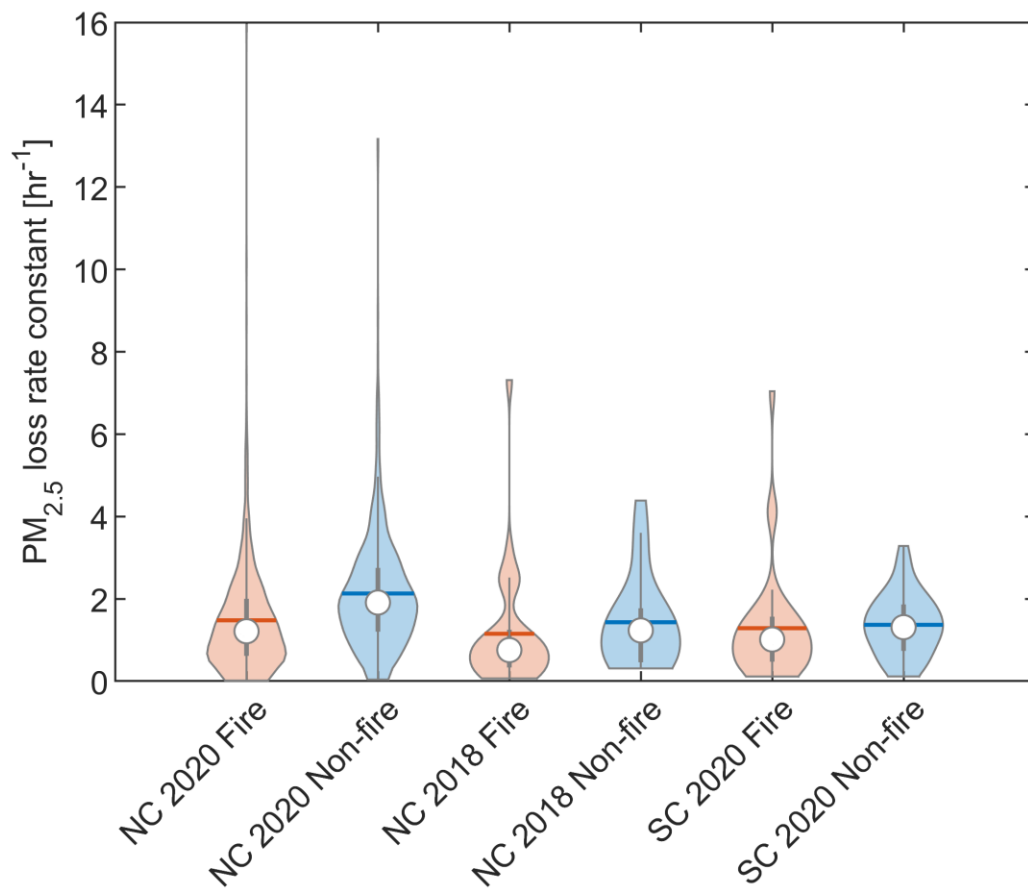


Fig. S11. Infiltration ratio on fire days for cool buildings (95th percentile indoor temperature < 30°C, $N = 142$) and hot buildings (95th percentile indoor temperature $\geq 30^\circ\text{C}$, $N = 1132$) in the San Francisco Bay Area in August and September 2020. The cool buildings have significantly lower fire-day infiltration ratios than the hot ones ($p < 0.01$), and 17% of cool buildings had extremely low infiltration ratios (< 0.1).



830 **Fig. S12.** Violin plot of total particle loss rate constant in buildings in on the fire days and non-fire days. NC = San Francisco Bay Area, SC = Los Angeles Area. Each violin plot shows the probability density of the total PM_{2.5} decay rate and a boxplot of interquartile range with whiskers extended to 1.5 times the interquartile range. Circles indicate the median, and horizontal lines indicate the mean.

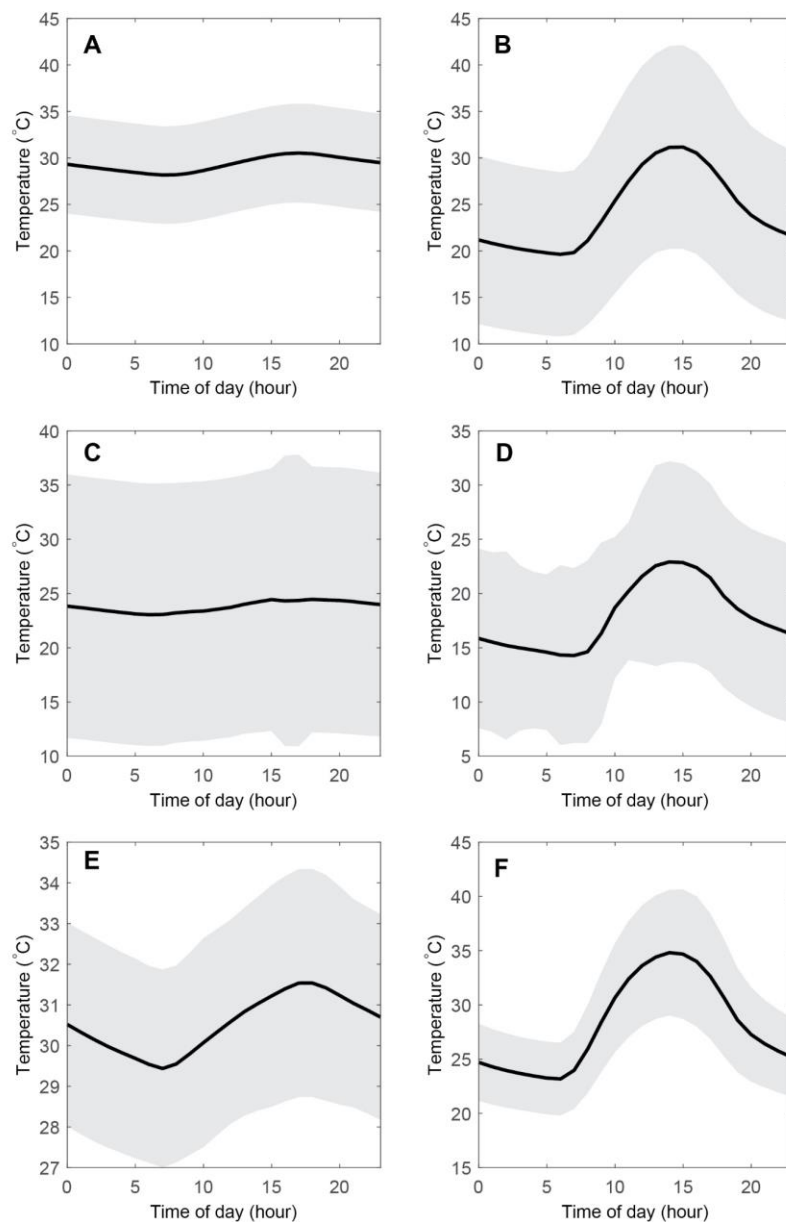


Fig. S13. Diel plots (local time) of average temperature measured by PurpleAir sensors in the San Francisco Bay Area in August-September 2020 (**A.** Indoor **B.** Outdoor) and November 2018 (**C.** Indoor **D.** Outdoor); and in August-September 2020 in Greater Los Angeles Area (**E.** Indoor **F.** Outdoor). Gray shading shows the standard deviation. In the Summer 2020 cases, the difference in daytime indoor/outdoor temperature alternated between positive and negative values. In the NC November 2018 case, the indoor temperature was almost always higher than the outdoor temperature.

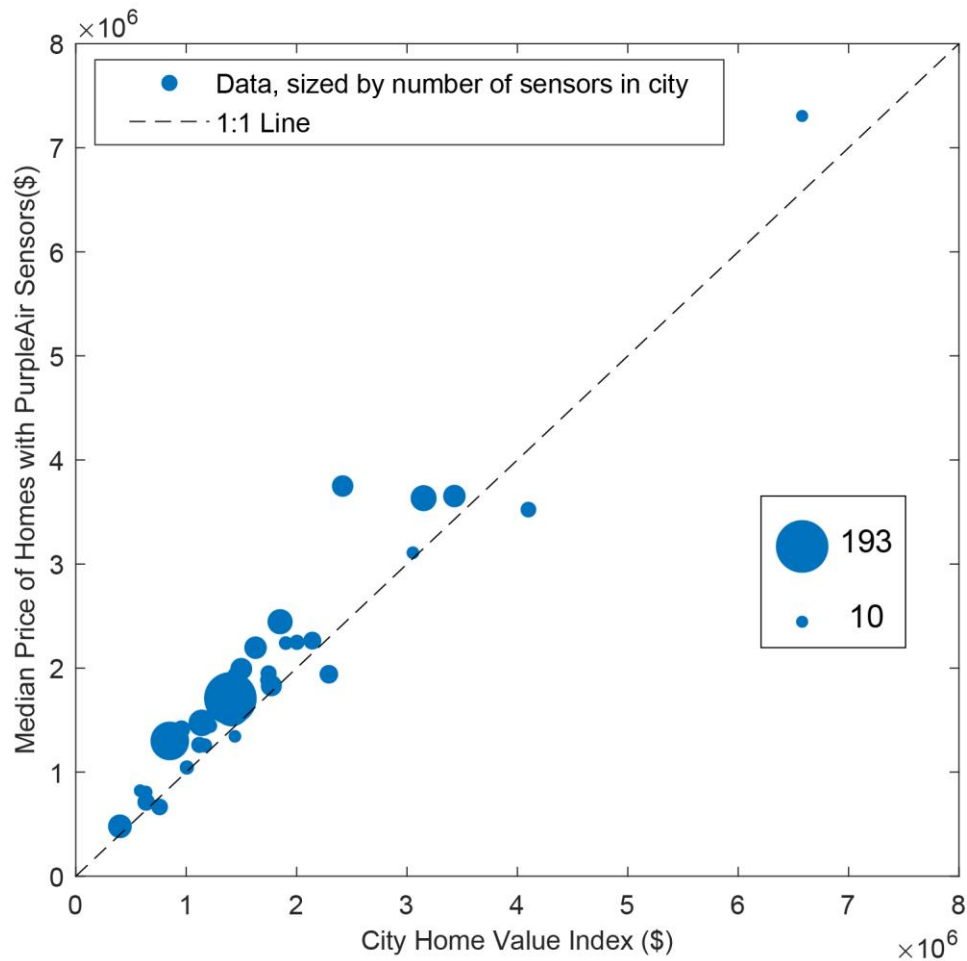


Fig. S14. Median price of homes with indoor PurpleAir sensors vs. Median Housing Price in that city, sized by the number of indoor sensors in that city (only showing data from cities with at least 10 buildings with valid indoor sensors in the NC 2020 case). PurpleAir owners live in homes with estimated average property values 21% greater than the median property value for their cities.

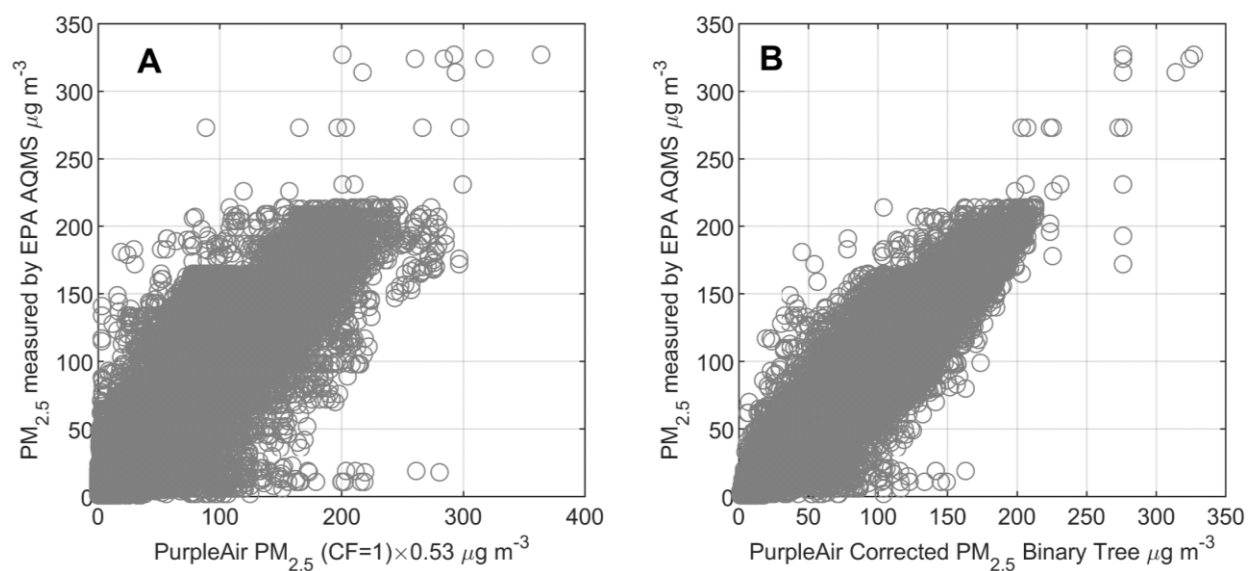


Fig. S15. A. Hourly PM_{2.5} measured by EPA AQMS against the linearly corrected (correction factor = 0.53) PM_{2.5} data measured by nearby PurpleAir sensors; **B.** Hourly PM_{2.5} measured by EPA AQMS against PM_{2.5} measured by the PurpleAir sensors after the binary tree correction, both for data in San Francisco Bay Area in August and September 2020. This figure demonstrates the binary tree model can improve the precision and accuracy of the sensors.

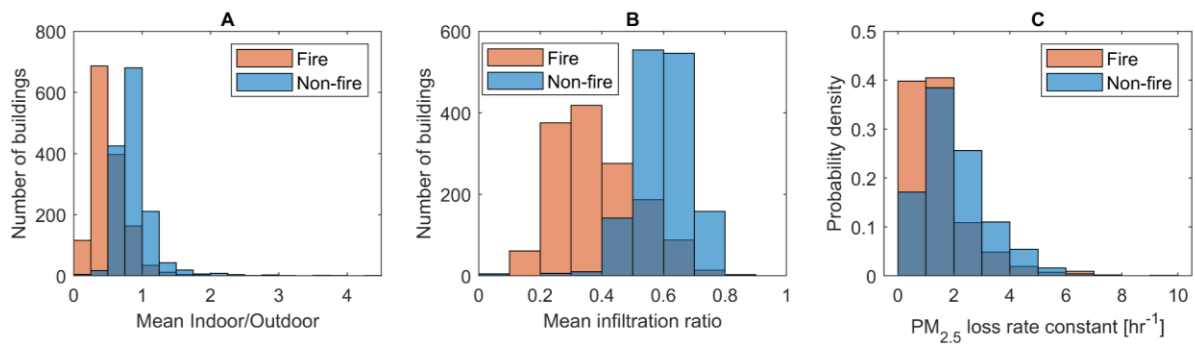
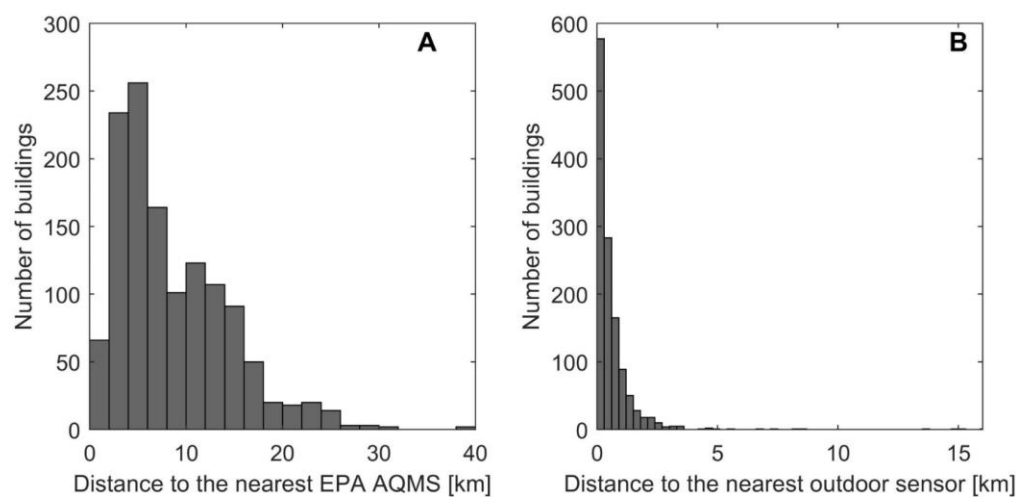
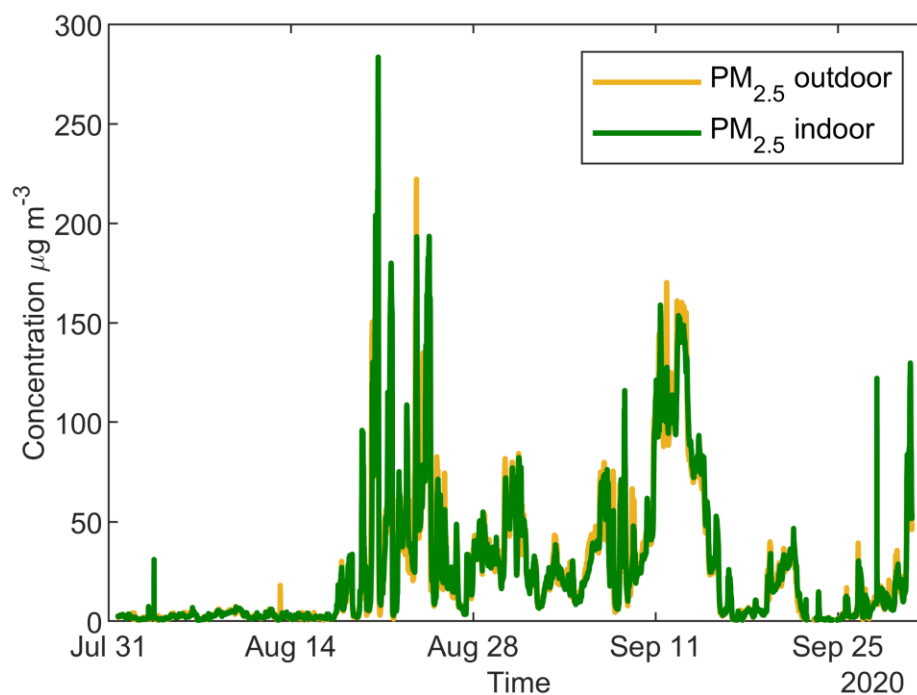


Fig. S16. Binary tree PM_{2.5} correction case. **A.** Distribution of mean Indoor/Outdoor PM_{2.5} ratio during fire days and non-fire days for the buildings; **B.** Distribution of Infiltrated/Outdoor PM_{2.5} ratio during fire days and non-fire days for the buildings. **C.** Probability density distribution of total indoor particle loss rate constants of PM_{2.5} for the NC 2020 case. This figure demonstrates the binary tree correction does not meaningfully affect the fire day/non-fire day comparison.



865 **Fig. S17.** Distribution of distance from the indoor sensor to **A.** the nearest EPA air quality measurement station and **B.** the nearest outdoor PurpleAir sensor in the NC 2020 case. The geometric mean (GM) distance from an indoor sensor to the nearest AQMS is 6.7 km, but it is only 0.21 km to the nearest outdoor PurpleAir sensor.



870

Fig. S18. Concentration timelines of PM_{2.5} reported by an “indoor” sensor and the nearest outdoor sensor. Because the indoor concentration measured is too close to and too well correlated with the outdoor concentration, this sensor might be placed outdoors. This node was therefore not used in this analysis.

Table S1. Parameters and performance of 7 correction methods for the outdoor sensors in the San Francisco Bay Area in August and September 2020 (NC 2020 case). Parameters are for the correction equation $PM_{2.5,corrected} = \beta_0 + \beta_1 PM_{CF1} + \beta_2 RH$. RH is between 0 and 1.

	Linear regression with intercept	Linear regression no intercept	Linear regression no intercept (ODR)	Barkjohn et al.(9) US fire correction	Holder et al. (3) wildfire correction	New fit incorporating RH	Binary decision tree with RH
β_0 [$\mu\text{g m}^{-3}$]	3.52	n/a	n/a	5.60	-3.21	3.92	n/a
β_1	0.50	0.53	0.54	0.53	0.51	0.50	n/a
β_2	n/a	n/a	n/a	-0.084	n/a	-0.80	n/a
RMSE ^a [$\mu\text{g m}^{-3}$]	12.2	12.6	12.6	12.8	13.9	12.2	7.7
NRMSE ^b	0.48	0.50	0.50	0.51	0.55	0.48	0.39
Regression R^2	0.88	n/a	n/a	n/a	n/a	n/a	n/a
R^2 of calibrated data against EPA reference measurements	0.88	0.87	0.87	0.88	0.88	0.88	0.95

a. The root mean square error (RMSE, in [$\mu\text{g m}^{-3}$]) is calculated by

$$RMSE = \sqrt{\frac{1}{N} \sum_{h=1}^N (x_h - R_h)^2},$$

where N is the number of 1-hour $PM_{2.5}$ [$\mu\text{g m}^{-3}$] data points. x_h is hourly averaged sensor $PM_{2.5}$ concentration [$\mu\text{g m}^{-3}$] for hour h after correction. R_h is the hourly concentration of $PM_{2.5}$ [$\mu\text{g m}^{-3}$] measured by the EPA AQMS.

b. The root mean squared error normalized to the observed mean (NRMSE) is calculated by:

$$NRMSE = \frac{RMSE}{\overline{R_h}},$$

where R_h is the mean $\text{PM}_{2.5}$ [$\mu\text{g m}^{-3}$] observed by reference EPA AQMS.

Table S2. Corrections based on linear regression of EPA monitor PM_{2.5} measurements with PurpleAir Sensors within certain distance in the San Francisco Bay Area in August and September 2020 (NC 2020 case). Number of sensors refer to the total number of sensors near EPA monitoring sites that meets the requirements described in the “Selection of correction method” section in the Supplement. At most 50 sensors near each EPA site were included. Parameters are for the correction equation.

Distance (km)	2	5	10	20
Number of sensors	104	442	624	750
Intercept $\beta_0 \neq 0$				
β_0 [$\mu\text{g m}^{-3}$]	3.26	3.52	3.77	4.05
β_1	0.50	0.50	0.50	0.49
R^2	0.89	0.88	0.87	0.85
RMSE [$\mu\text{g m}^{-3}$]	11.5	12.2	12.7	13.5
NRMSE	0.46	0.49	0.51	0.53
No intercept ($\beta_0 = 0$)				
β_1	0.53	0.53	0.51	0.52
R^2	n/a	n/a	n/a	n/a
RMSE [$\mu\text{g m}^{-3}$]	11.8	12.6	13.1	13.9
NRMSE	0.47	0.50	0.52	0.55

Table S3. Median prices of homes with PurpleAir sensors compared to Home Value Index in cities with at least 10 buildings with valid indoor sensors in the NC 2020 case, as of December 2020.

Prices were rounded to nearest thousand.

	Median price of homes with PurpleAir sensors	Number of buildings with PurpleAir sensors	Zillow Home Value Index of that city	Price Difference ^a
Alameda	\$1,143,000	18	\$1,119,000	2%
Albany	\$1,257,000	14	\$1,170,000	7%
Atherton	\$7,306,000	10	\$6,579,000	11%
Belmont	\$2,240,000	13	\$1,902,000	18%
Berkeley	\$1,616,000	93	\$1,411,000	14%
Campbell	\$1,344,000	11	\$1,441,000	-7%
Davis	\$666,000	19	\$759,000	-12%
El Cerrito	\$1,045,000	14	\$ 1,006,000	4%
Emeryville	\$822,000	11	\$ 583,000	41%
Lafayette	\$1,992,000	33	\$ 1,499,000	33%
Los Altos	\$3,653,000	35	\$ 3,429,000	7%
Los Gatos	\$2,264,000	22	\$ 2,142,000	6%
Menlo Park	\$3,645,000	32	\$2,417,000	51%
Mill Valley	\$1,911,000	18	\$1,746,000	9%
Moraga	\$1,886,000	11	\$1,726,000	9%
Mountain View	\$2,317,000	44	\$1,851,000	25%
Oakland	\$1,300,000	104	\$851,000	53%
Orinda	\$1,941,000	24	\$2,292,000	-15%
Palo Alto	\$3,594,000	47	\$3,151,000	14%
Portola Valley	\$3,523,000	17	\$4,099,000	-14%
Redwood City	\$2,196,000	35	\$1,628,000	35%
Richmond	\$807,000	12	\$635,000	27%
Sacramento	\$469,000	39	\$400,000	17%
San Carlos	\$2,248,000	16	\$2,003,000	12%
San Francisco	\$1,696,000	193	\$1,400,000	21%
San Jose	\$1,460,000	49	\$1,141,000	28%
San Mateo	\$1,919,000	28	\$1,461,000	31%
San Rafael	\$1,447,000	15	\$1,214,000	19%
Santa Rosa	\$713,000	21	\$637,000	12%
Saratoga	\$3,109,000	11	\$3,053,000	2%
Sunnyvale	\$1,654,000	31	\$1,771,000	-7%
Walnut Creek	\$1,414,000	21	\$958,000	48%

^aPrice difference = (Median price of homes with PurpleAir sensors - Median City Home Value)/

Median City Home Value

Table S4. Mean \pm standard deviation of fire-day infiltration ratios and the number of buildings with fire-day infiltration ratios below 0.14 or above 0.40 in cities with at least 10 buildings with valid indoor sensors in the NC 2020 case.

City	Number of buildings with PurpleAir sensors	Mean \pm SD of Fire-day infiltration ratio	No. of Buildings with Fire-day infiltration ratio < 0.14	No. of Buildings with Fire-day infiltration ratio > 0.40
Alameda	18	0.19 \pm 0.09	5	1
Albany	14	0.31 \pm 0.11	0	3
Atherton	10	0.31 \pm 0.12	1	3
Belmont	13	0.27 \pm 0.08	1	1
Berkeley	93	0.27 \pm 0.10	10	13
Campbell	11	0.24 \pm 0.13	0	2
Davis	19	0.17 \pm 0.16	11	2
El Cerrito	14	0.27 \pm 0.10	2	1
Emeryville	11	0.26 \pm 0.16	3	1
Lafayette	33	0.23 \pm 0.11	5	4
Los Altos	35	0.33 \pm 0.19	7	12
Los Gatos	22	0.34 \pm 0.15	2	7
Menlo Park	32	0.27 \pm 0.12	3	5
Mill Valley	18	0.36 \pm 0.18	1	6
Moraga	11	0.16 \pm 0.10	4	0
Mountain View	44	0.25 \pm 0.14	12	5
Oakland	104	0.25 \pm 0.12	14	11
Orinda	24	0.24 \pm 0.19	11	5
Palo Alto	47	0.28 \pm 0.17	12	15
Portola Valley	17	0.27 \pm 0.12	2	3
Redwood City	35	0.30 \pm 0.15	8	11
Richmond	12	0.25 \pm 0.16	4	2
Sacramento	39	0.29 \pm 0.19	10	10
San Carlos	16	0.20 \pm 0.10	5	1
San Francisco	193	0.28 \pm 0.12	24	35
San Jose	49	0.26 \pm 0.14	14	10
San Mateo	28	0.26 \pm 0.11	3	2
San Rafael	15	0.31 \pm 0.16	3	5
Santa Rosa	21	0.31 \pm 0.15	4	6
Saratoga	11	0.30 \pm 0.18	0	2
Sunnyvale	31	0.22 \pm 0.15	8	7
Walnut Creek	21	0.21 \pm 0.14	9	1

Table S5. Weibull parameters of the concentration indoor/outdoor ratios for buildings with PurpleAir sensors in August-September 2020 in the San Francisco Bay Area (35 $\mu\text{g m}^{-3}$ daily average $\text{PM}_{2.5}$ concentration measured at the nearest EPA measurement site was used as the threshold for fire days and non-fire days). $N = 1274$. Unhealthy days are defined as days with daily average EPA $\text{PM}_{2.5}$ concentration above 55.4 $\mu\text{g/m}^3$.

	Mean indoor conc $\mu\text{g m}^{-3}$		Indoor/outdoor ratio		Infiltration ratio	
	γ	β	γ	β	γ	β
Non-fire days	4.65	1.82	1.00	1.35	1.00	1.35
Fire days	12.4	1.50	0.45	1.26	0.30	2.00
Unhealthy days	14.9	1.40	0.34	1.19	0.26	1.74

Quantile-quantile plots (*SI Appendix*, Fig. S4) show the mean concentration of indoor $\text{PM}_{2.5}$ in all the buildings can be satisfactorily described by the Weibull distribution. The scale parameter and shape parameter of the Weibull fit are γ and β , respectively. The probability distribution function for

x is $f(x) = \frac{\beta}{\gamma} \left(\frac{x}{\gamma}\right)^{\beta-1} e^{-(x/\gamma)^\beta}$, where $x > 0$. Parameters of the SC 2020 and NC 2018 cases are not

shown here due to the small sample sizes, which are less representative of all the buildings in these areas at that time.

SI References

1. T. Sayahi, A. Butterfield, K. E. Kelly, Long-term field evaluation of the Plantower PMS low-cost particulate matter sensors. *Environ. Pollut.* **245**, 932–940 (2019).
2. W. W. Delp, B. C. Singer, Wildfire smoke adjustment factors for low-cost and professional PM2.5 monitors with optical sensors. *Sensors* **20**, 1–21 (2020).
3. A. L. Holder, *et al.*, Field evaluation of low-cost particulate matter sensors for measuring wildfire smoke. *Sensors* **20**, 1–17 (2020).
4. K. Ardon-Dryer, Y. Dryer, J. N. Williams, N. Moghimi, Measurements of PM2.5 with PurpleAir under atmospheric conditions. *Atmos. Meas. Tech.* **13**, 5441–5458 (2020).
5. T. Zheng, *et al.*, Field evaluation of low-cost particulate matter sensors in high-and low-concentration environments. *Atmos. Meas. Tech.* **11**, 4823–4846 (2018).
6. K. K. Barkjohn, B. Gantt, A. L. Clements, Development and Application of a United States wide correction for PM2.5 data collected with the PurpleAir sensor. *Atmos. Meas. Tech. Discuss.* (2020) <https://doi.org/10.5194/amt-2020-413> (January 5, 2021).
7. J. Bi, A. Wildani, H. H. Chang, Y. Liu, Incorporating Low-Cost Sensor Measurements into High-Resolution PM2.5 Modeling at a Large Spatial Scale. *Environ. Sci. Technol.* **54**, 2152–2162 (2020).
8. K. K. Barkjohn, *et al.*, Real-time measurements of PM2.5 and ozone to assess the effectiveness of residential indoor air filtration in Shanghai homes. *Indoor Air* **31**, 74–87 (2021).
9. K. K. Barkjohn, A. Holder, S. Frederick, G. Hagler, A. Clements, PurpleAir PM2.5 U.S. Correction and Performance During Smoke Events in *International Smoke Symposium*, (2020).
10. K. E. Kelly, *et al.*, Ambient and laboratory evaluation of a low-cost particulate matter

- sensor. *Environ. Pollut.* **221**, 491–500 (2017).
11. C. Malings, *et al.*, Fine particle mass monitoring with low-cost sensors: Corrections and long-term performance evaluation. *Aerosol Sci. Technol.* **54**, 160–174 (2020).
 12. M. Levy Zamora, *et al.*, Field and Laboratory Evaluations of the Low-Cost Plantower Particulate Matter Sensor. *Environ. Sci. Technol.* **53**, 838–849 (2019).
 13. C. Wu, J. Zhen Yu, Evaluation of linear regression techniques for atmospheric applications: The importance of appropriate weighting. *Atmos. Meas. Tech.* **11**, 1233–1250 (2018).
 14. J. Bi, L. A. Wallace, J. A. Sarnat, Y. Liu, Characterizing outdoor infiltration and indoor contribution of PM_{2.5} with citizen-based low-cost monitoring data. *Environ. Pollut.* **276** (2021).
 15. P. Tiitta, *et al.*, Measurements and modelling of PM_{2.5} concentrations near a major road in Kuopio, Finland. *Atmos. Environ.* **36**, 4057–4068 (2002).
 16. T. Suvendrini Lena, V. Ochieng, M. Carter, J. Holguín-Veras, P. L. Kinney, Elemental carbon and PM_{2.5} levels in an urban community heavily impacted by truck traffic. *Environ. Health Perspect.* **110**, 1009–1015 (2002).
 17. A. A. Karner, D. S. Eisinger, D. A. Niemeier, Near-roadway air quality: Synthesizing the findings from real-world data. *Environ. Sci. Technol.* **44**, 5334–5344 (2010).
 18. J. S. Apte, *et al.*, High-Resolution Air Pollution Mapping with Google Street View Cars: Exploiting Big Data. *Environ. Sci. Technol.* **51**, 6999–7008 (2017).
 19. R. Allen, T. Larson, L. Sheppard, L. Wallace, L. J. S. Liu, Use of real-time light scattering data to estimate the contribution of infiltrated and indoor-generated particles to indoor air. *Environ. Sci. Technol.* **37**, 3484–3492 (2003).

20. R. Allen, L. Wallace, T. Larson, L. Sheppard, L. J. S. Liu, Estimated hourly personal exposures to ambient and nonambient particulate matter among sensitive populations in seattle, washington. *J. Air Waste Manag. Assoc.* **54**, 1197–1211 (2004).
21. S. Patel, *et al.*, Indoor Particulate Matter during HOMEChem: Concentrations, Size Distributions, and Exposures. *Environ. Sci. Technol.* **54**, 7107–7116 (2020).
22. C. Chen, B. Zhao, Review of relationship between indoor and outdoor particles: I/O ratio, infiltration factor and penetration factor. *Atmos. Environ.* **45**, 275–288 (2011).
23. L. Wallace, R. Williams, Use of personal-indoor-outdoor sulfur concentrations to estimate the infiltration factor and outdoor exposure factor for individual homes and persons. *Environ. Sci. Technol.* **39**, 1707–1714 (2005).
24. S. Bhangar, N. A. Mullen, S. V Hering, N. M. Kreisberg, W. W. Nazaroff, Ultrafine particle concentrations and exposures in seven residences in northern California. *Indoor Air* **21**, 132–144 (2011).
25. W. Ott, L. Wallace, D. Mage, Predicting particulate (PM10) personal exposure distributions using a random component superposition statistical model. *J. Air Waste Manag. Assoc.* **50**, 1390–1406 (2000).
26. B. Stephens, J. A. Siegel, Penetration of ambient submicron particles into single-family residences and associations with building characteristics. *Indoor Air* **22**, 501–513 (2012).
27. California Energy Commission, *California Building Climate Zone Areas* (2018) (January 26, 2021).